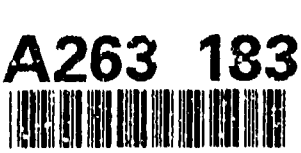

(2)

ARMY RESEARCH LABORATORY

Electromagnetic Diffusion and Wire Coupling

by Bart Goldstein and
Rudolf Goldflam

ARL-CR-54 April 1993

prepared by

Mission Research Corporation
735 State Street
P.O. Drawer 719
Santa Barbara, CA 93101

under contract

DAAL02-87-C0113

The findings in this report are not to be construed as an official Department of the Army position unless so designated by other authorized documents.

Citation of manufacturer's or trade names does not constitute an official endorsement or approval of the use thereof.

Destroy this report when it is no longer needed. Do not return it to the originator.

TABLE OF CONTENTS

TABLE OF CONTENTS (CONCLUDED)

LIST OF ILLUSTRATIONS

LIST OF ILLUSTRATIONS (CONCLUDED)

LIST OF TABLES

SECTION 1

INTRODUCTION AND SUMMARY OF RESULTS

1.1 Statement of the Problem

Electromagnetic radiation can diffuse through a thin walled metallic enclosure and, perhaps, interfere with the proper functioning of internal electronics. This report shows how to predict the current induced on a wire within a rectangular metallic box (figure 1) which is irradiated with an electromagnetic pulse. The wire is connected between opposite walls of the box and the incident pulse has arbitrary time history and angle of incidence. Simple formulas are derived for a straight wire. The case of an arbitrarily shaped wire within any shape enclosure is discussed semi-quantitatively. Good agreement has been found between the analytic formulas and computer code results.

This work was motivated by an experiment at Harry Diamond Laboratory which measured the current produced on a wire within a shielded room by an EMP simulator. The walls of the room were entirely coated with metal so that diffusion was the primary mechanism for leakage of radiation into the enclosure. A future document will compare the results of these experiments with the theory developed in this report. Comparisons are shown here between the theory and some code results.

It is helpful to consider three distinct regimes in frequency space[1-5]. In the low frequency regime the skin depth is larger than the wall thickness of the enclosure. For instance, if the conductivity and wall thickness of the enclosure are 10^6 and 1 millimeter, respectively, then the low frequency regime extends from zero frequency to about 1.6×10^6 Hertz (angular frequency). The intermediate frequency regime extends up to the frequency of the lowest internal mode of the enclosure. For example, the lowest mode of a cube two meters on each side is 2.5×10^8 Hertz. The high frequency regime extends upward from the lowest mode.

Figures 2, 3, and 4 show typical results yielded by the theory. Figures 2, 3 and 4a show the wire current as a function of the frequency of the incident pulse in the low, intermediate and high frequency regimes for a box 2 meters on each side irradiated with an external field of H_x=1 Ampere/meter. The wire parameters and other details are indicated in sections 1.2 - 1.4. As expected, the wire current is largest at low frequencies

because the enclosure is a good shield if the skin depth is smaller than the wall thickness. Figure 4b shows the wire current in the time domain. The box is irradiated by a ten nanosecond long square pulse whose magnetic field rises abruptly to a peak H_x=1000 Amperes/meter. The wire current rises to a peak value of about 0.5 ma which persists for about 100 microseconds. The wire resistance is 0.01 ohms/meter and the inductance is 10^{-6} henry/meter. The other parameters are the same as in the calculations of figures 2-4.

The remainder of this introduction (sections 1.2, 1.3 and 1.4) summarizes the final results of this analysis. The final analytical formulas for the three regimes are discussed along with the code comparisons which corroborate them. Section 1.4 discusses the physics of the wire response and extends the analysis to arbitrarily shaped enclosures and wire shapes. Section 1.5 summarizes some basic mathematical facts which are used in sections 2–5. Sections 2 through 5 contain the detailed derivations of the results summarized in section 1. Section 6 discusses the code HFC which treats external scattering from a box. A previous report discusses the low frequency regime in greater detail. For the reader's convenience it is reproduced here (with some minor corrections) in Appendix A.

MKS units are used in this report.

1.2 Low Frequency Regime

This subsection summarizes the final results of the low frequency regime. The detailed derivation are shown in Appendix A.

For boxes of any practical size the wavelength of the incident electromagnetic wave in the low frequency regime is much larger than the box. Consequently, in the neighborhood of the box the incident magnetic field is spatially uniform and is given by the real part of

$$H^D e^{-i\omega t} \quad . \qquad (1--1)$$

Here, a single Fourier component of the incident pulse will be considered which oscillates at the frequency ω. The time domain wire current will be considered below.

The uniform external field can be resolved into its vector components H_x^D, H_y^D and H_z^D along the three axes in figure 1. Then the current in the wire is given by the final result

$$I(\omega) = \frac{i\omega\mu_0 H_x^e}{\gamma - i\omega L}(z_0 - \frac{c}{2})\frac{b}{b+c} - \frac{i\omega\mu_0 H_z^e}{\gamma - i\omega L}(x_0 - \frac{a}{2})\frac{b}{a+b} \quad . \qquad (1-2)$$

Here, the coordinates of the wire are $x = x_0$ and $z = z_0$. H_x^e and H_z^e are the vector components of the magnetic field inside the box

$$H_x^e = \frac{H_x^D}{1 - i\omega/\omega_1}$$

$$H_z^e = \frac{H_z^D}{1 - i\omega/\omega_1} \qquad (1\text{-}3)$$

which are also spatially uniform (Appendix A and section 2). Also a,b,c are the box dimensions and

$$\bar{a} = \left(\frac{3abc}{4\pi}\right)^{1/3} \quad .$$

The resistance per unit length of the wire (at zero frequency) is, of course[6],

$$R_0 = \frac{1}{\pi w_0^2 \sigma_0}(\frac{ohm}{meter}) \qquad (1-4)$$

in terms of its radius w_0 and conductivity σ_0. But at higher frequency where the skin depth

$$\delta_0 = \sqrt{\frac{2}{\mu_0\omega\sigma_0}} \qquad (1-5)$$

is less than the wire radius ($\delta_0 < w_0$) the wire impedance[6] is

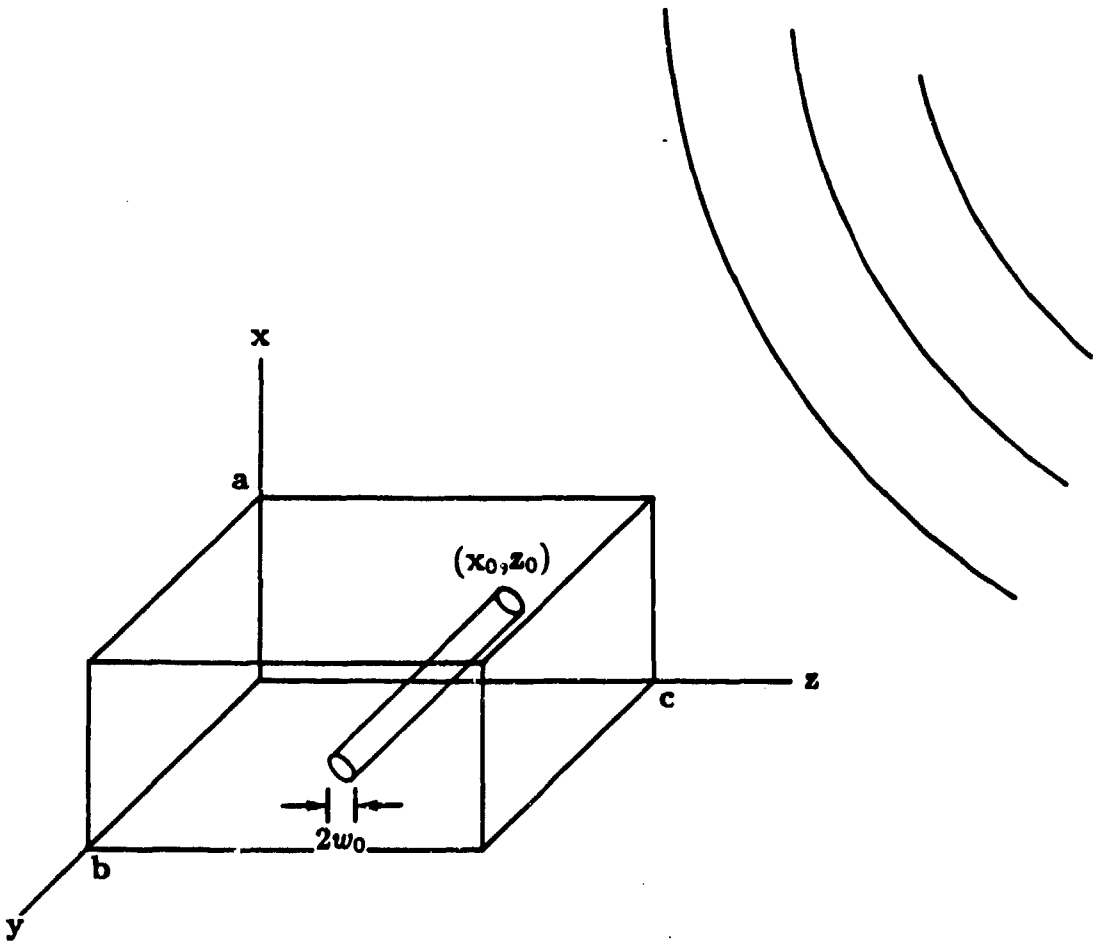

Figure 1. Problem geometry.

$$R_0(1-i)\frac{w_0}{2\delta_0}\left(\frac{ohm}{meter}\right) \quad . \tag{1-6}$$

The symbol γ is defined to be

$$\gamma = \begin{cases} R_0 & \text{if } \delta_0 \leq w_0 \\ R_0(1-i)\frac{w_0}{2\delta_0} & \text{if } \delta_0 > w_0 \end{cases} \tag{1-7}$$

L is the inductance per unit length of the wire in the box. Above the frequency

$$\omega_1 = \frac{3}{\mu_0 \sigma \Delta \bar{a}} \tag{1-8}$$

where σ and Δ are the wall conductivity and thickness the inductance is

$$L = \frac{8\mu_0}{ac\pi^2} \sum_{\ell,n=1}^{\infty} \frac{\sin^2\left(\frac{\ell\pi x_0}{a}\right)\sin^2\left(\frac{n\pi z_0}{c}\right)}{\left(\frac{\ell}{a}\right)^2 + \left(\frac{n}{c}\right)^2} \quad \left(\frac{henry}{meter}\right) \quad . \tag{1-9}$$

Below this frequency it is approximately the inductance which the wire would have in free space outside the box. The symbols μ_0 and ϵ_0 have their usual meaning.

Figure 2 compares the wire current predicted by equation 1-2 with the current computed by the computer code BOX4 discussed in Appendix A. The agreement is within a factor of four over five orders of magnitude of frequency. In this example the box is two meters on each side and the walls are one millimeter thick. The wall conductivity is 10^6 mho/meter. The wire resistance $R_0 = 0.0183$ ohm/meter and it is located one-half meter from the $x = 0$ and $z = 0$ walls. The wire is one centimeter in radius and the external magnetic field is pointing in the x - direction and has a magnitude on one ampere/meter.

Table 1 indicates that the wire current is predicted at different positions of the wire at one hertz angular frequency. Agreement is within twenty percent when the wire location is varied from $z_0 = 0.05$ to $z_0 = 0.95$ meters. All other parameters are identical to the figure 2 case.

Table 1. Wire current as a function of wire position.

Wire Position x (cm)	Wire Current Theory (Amp)	Wire Current Code (Amp)
5	3.3×10^{-5}	3.5×10^{-5}
10	3.1×10^{-5}	3.3×10^{-5}
50	1.7×10^{-5}	1.6×10^{-5}
95	1.7×10^{-6}	1.4×10^{-6}

Tabie 2 indicates good agreement between the analytic expressiors and the code when the frequency is 10^5 hertz. The analysis always underpredicts the current by about of factor of three.

Table 2. Wire current as a function of wire position.

Wire Position x (cm)	Wire Current Theory (Amp)	Wire Current Code (Amp)	Ratio Code ÷ Theory
5	0.033	0.10	3.0
10	0.027	0.081	3.0
50	0.011	0.043	3.9
95	0.0011	0.0029	2.6

Figure 2 illustrates the general behavior of the wire current. It increases linearly with frequency to a peak value. At sufficiently high frequency the inductive reactance of the wire becomes large enough to cause the current to decrease.

The wire current can be obtained as a function of time by taking the inverse fourier transform of equation 1-2. If the incident pulse has an arbitrary time history given by the function $H^D_{(t)}$ then the wire current is

$$I(t) = \frac{\mu_0 \omega_1 (z_0 - \frac{\varsigma}{2}) \frac{b}{b+c}}{R_0 - \omega_1 L} \int_0^t dt' H_x^D \left\{ \frac{R}{L} e^{-\frac{R}{L}(t-t')} - \omega_1 e^{-\omega_1 (t-t')} \right\}$$

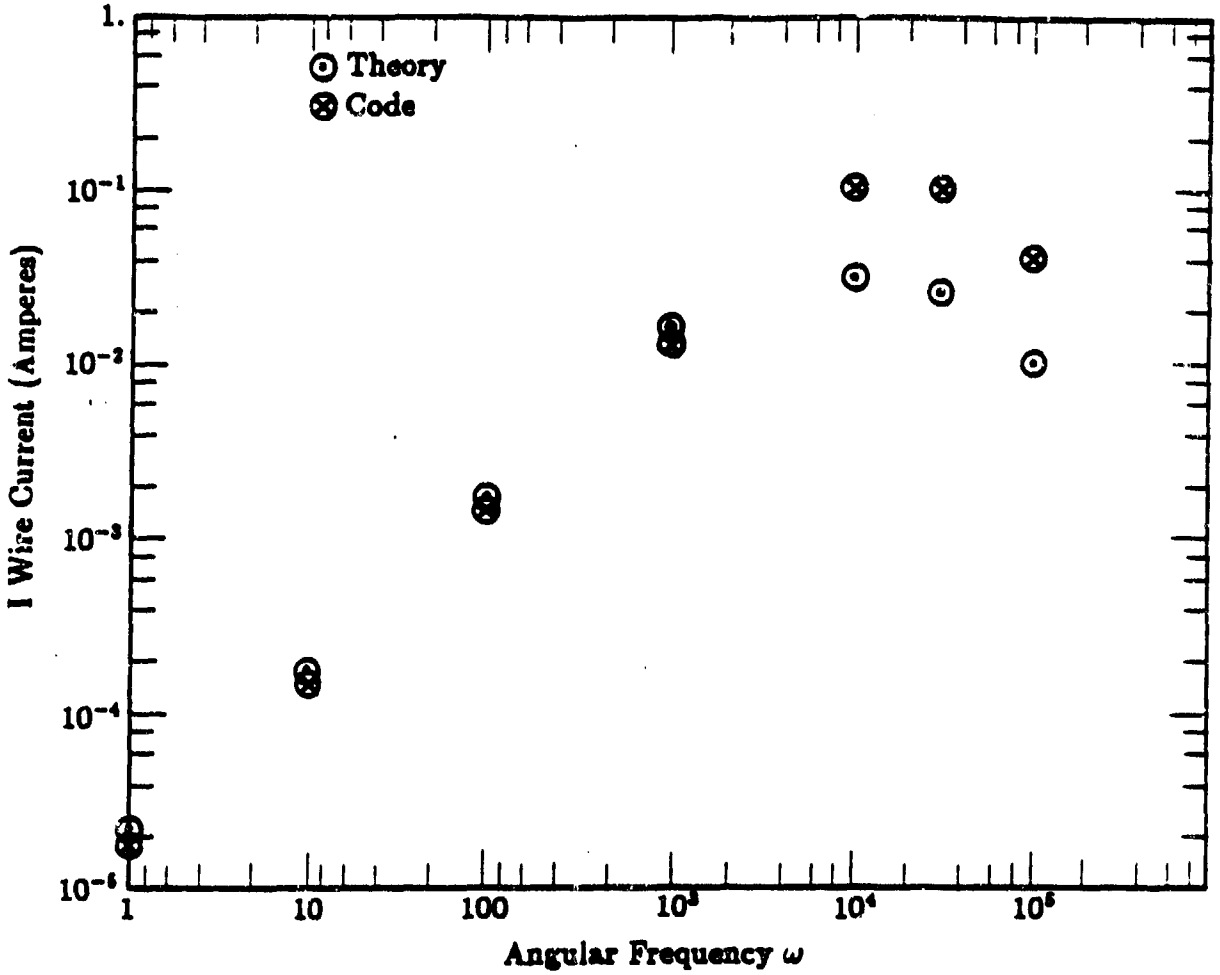

Figure 2. Wire current.

$$- \frac{\mu_0 \omega_1 (x_0 - \frac{a}{2}) \frac{b}{a+b}}{R_0 - \omega_1 L} \int_0^t dt' H_z^D \left\{ \frac{R}{L} e^{-\frac{R}{L}(t-t')} - \omega_1 e^{-\omega_1 (t-t')} \right\} \text{(Amp)} \qquad (1\text{-}10)$$

In general, this integral smoothes out the fluctuations in the incident pulse so that the wire current is much less rapidly varying. When the incident pulse first reaches the box the wire current slowly builds and after the pulse has past the box the wire current slowly decays to zero.

These results are explained in section 2 and Appendix A.

1.3 Intermediate Frequency

The analytical formulas for the wire current in the intermediate frequency regime are summarized here. The details are in section 2.

In the intermediate frequency regime equation 1-2 applies but the internal magnetic fields within the box are no longer given by equation 1-3. Instead, the appropriate expressions to use are

$$H_x^e = \frac{H_x^D}{\cos(\beta\Delta) - \frac{1}{3}\beta\bar{a}\sin(\beta\Delta)}$$

$$H_z^e = \frac{H_z^D}{\cos(\beta\Delta) - \frac{1}{3}\beta\bar{a}\sin(\beta\Delta)} \quad . \qquad (1\text{-}11)$$

The wall thickness is Δ and the symbol β is the attenuation constant of a wave propagating in the metallic wall. In terms of the skin depth δ in the wall it is the complex number

$$\beta = \frac{1+i}{\delta} \qquad (1-12)$$

Figure 3 shows the intermediate frequency regime wire current for the case illustrated in figure 2. Clearly, at high frequency the wire current becomes very small because the walls are many skin depths thick and the enclosure is a good shield.

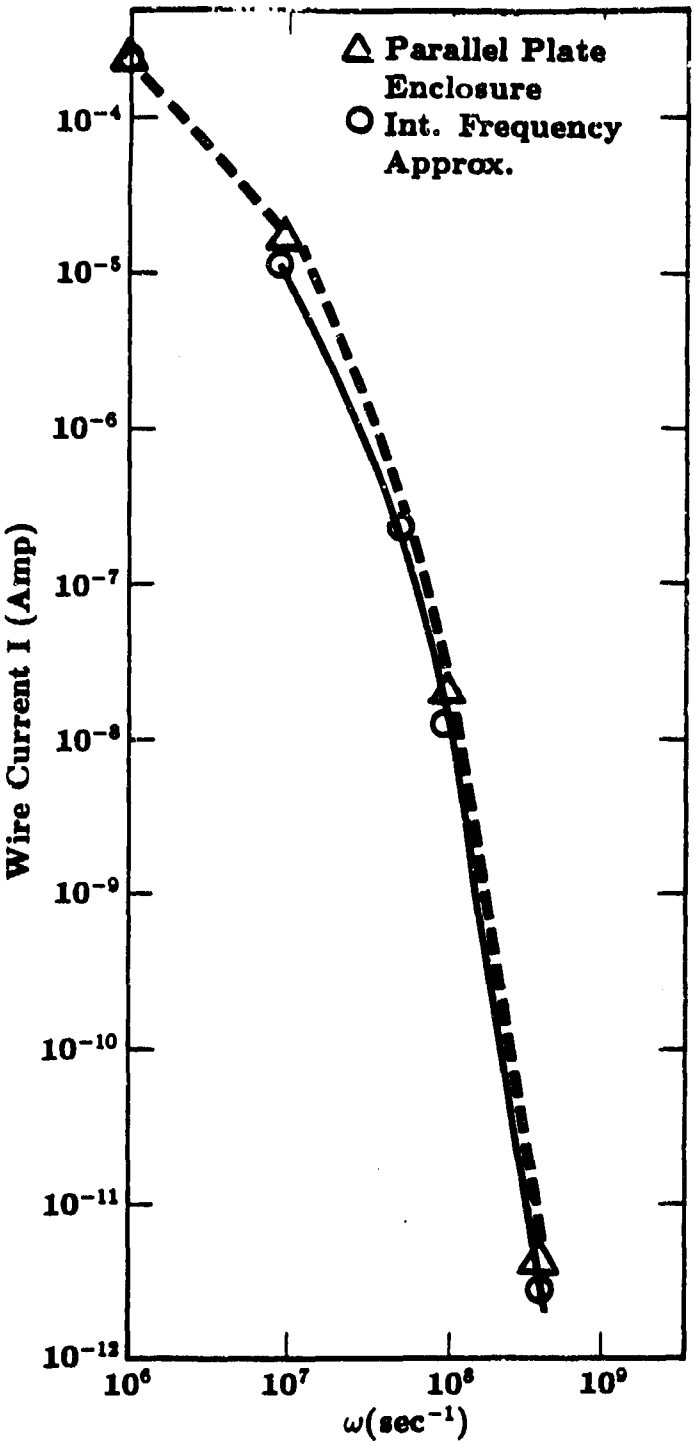

Figure 3. Intermediate frequency wire current.

The pulse starts to diffuse into the enclosure in a time $t_\Delta = \mu_0 \sigma \Delta^2$ seconds which is frequently many microseconds. If the incident pulsewidth is short compared to this time then the wire current in the time domain is approximately

$$I(t) = \frac{\mu_0}{L}\left[1 - \frac{4R_0 t}{L}\left(\frac{t}{t_\Delta}\right) + \frac{16R_0 t}{L}\left(\frac{t}{t_\Delta}\right)\right]\frac{2e^{-t_\Delta/4t}}{\sqrt{\pi}\xi_1 t_\Delta}\left(\frac{t_\Delta}{t}\right)^{1/2}$$

$$\left\{(z_0 - \frac{c}{2})\frac{b}{b+c}H_{0x} - (x_0 - \frac{a}{2})\frac{b}{a+b}H_{-s}\right\} \qquad t < t_\Delta/10$$

where $\xi_1 = \frac{\bar{a}}{3\Delta}$

$$I(t) = \frac{\mu_0 \omega_1}{R_0 - \omega_1 L}\left\{\frac{R_0}{L}e^{-R_0 t/L} - \omega_1 e^{-\omega_1 t}\right\}$$

$$\left\{(z_0 - \frac{c}{2})\frac{b}{b+c}H_{0x} - (x_0 - \frac{a}{2})\frac{b}{a+b}H_{0x}\right\} \qquad t \gg t_\Delta/10$$

The wire current does not depend upon the details of the time history of the incident pulse. Instead only the time integrated impulse

$$H_{0x} = \int_{-\infty}^{\infty} H_x^D dt$$

$$H_{0x} = \int_{-\infty}^{\infty} H_s^D dt$$

is important. The above early time approximation is valid provided $R_0 t_\Delta / 10L < 1$. In general, the wire current slowly rises to a peak at about the time $\tau_\Delta/10$. It then falls to zero. These expressions make use of the early and late time approximations for the internal magnetic field which was derived by Bedrosian and Lee[2,5].

1.4 High Frequency Regime

The analytic formulas for the high frequency wire current are summarized here.

If a plane wave is normally incident on the z = c wall of the box (figure 1) then the wire current is

$$I = \frac{\dfrac{-8Z_t H_x^i}{c^2} \displaystyle\sum_{\ell,n=1}^{\infty} \left\{ \frac{n(\cos n\pi)(1-\cos \ell\pi)}{\ell\left[(\frac{\ell\pi}{a})^2 + (\frac{n\pi}{c}) - k^2\right]} \right\} \sin\frac{\ell\pi x_0}{a} \sin\frac{n\pi z_0}{c}}{\gamma - \dfrac{4i\omega}{ac\epsilon_0 v^2} \displaystyle\sum_{\ell,n=1}^{\infty} \frac{\sin^2\frac{\ell\pi x_0}{a} \sin^2\frac{n\pi z_0}{c}}{(\frac{\ell\pi}{a})^2 + (\frac{n\pi}{c})^2 - k^2}} \qquad (1-13)$$

Here the incident wave magnetic field (at z = c)

$$H_x^i e^{-i\omega t} \qquad (1-14)$$

is in the x - direction and the transfer impedance of the wall is

$$Z_t = \frac{\beta}{\sigma \sin(\beta\Delta)} \quad . \qquad (1-15)$$

The speed of light in vacuum is denoted by v and $k = \omega/v$ is the wavenumber.

Figure 4 graphs the high frequency wire current given by equation 1-13 for the box referred to in the figures 2 and 3 example. As expected the wire current is minute. In the high frequency regime the incident frequency can equal the frequency of one of the internal modes of the box. One might expect that this would lead to a resonance which might cause a dramatic change in the wire current at the resonance frequency. Figure 4 shows one such resonance near 2 gigahertz angular frequency.

At low and intermediate frequencies the above formulas apply for any angle of incidence. However, the case of arbitrary angle of incidence at high frequency is much more complicated to treat and no simple formula applies. Instead a computational method has been derived. The code HFC (section 6) calculates the current on the outside of the box.

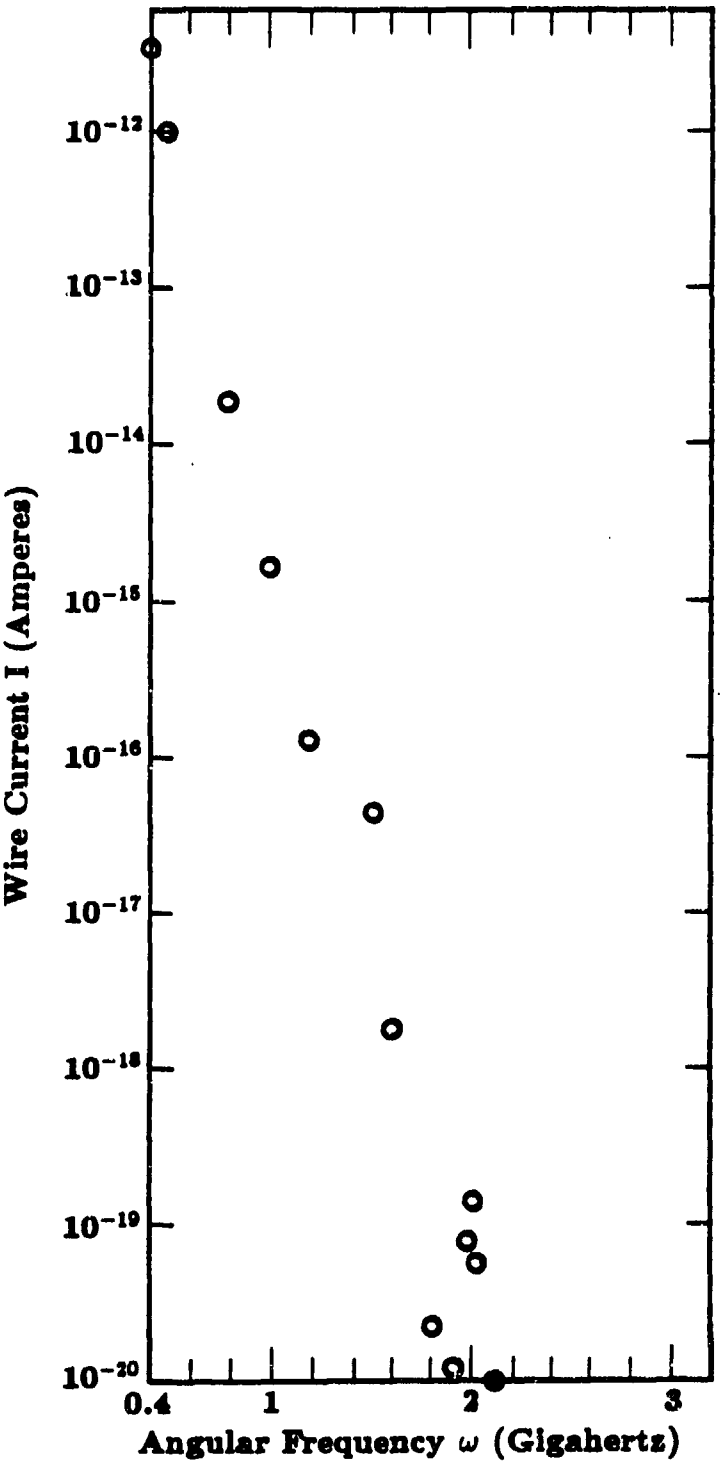

Figure 4a. High frequency wire current.

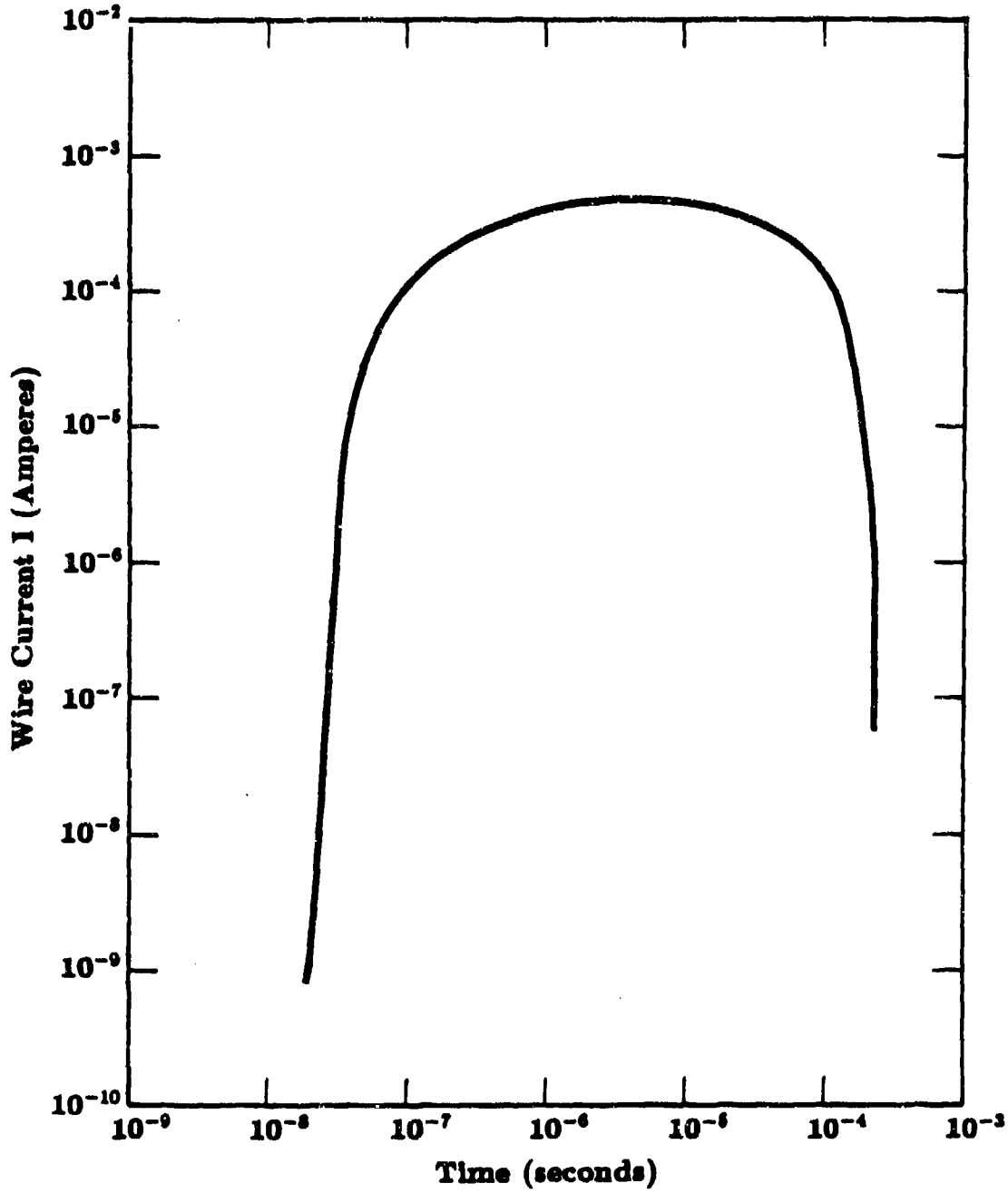

Figure 4b. Wire current versus time.

These results are then used by the method described in sections 4 and 5 to compute the wire current.

As a practical matter the wire current is so small at high frequencies that a very ...te prediction is probably not necessary. An approximate method which is convenient ...mploy is for most applications more useful. It is recommended that equation 1-13 be used to yield an approximation in the case that the frequency is so high that the wavelength of the incident wave is much less than the box dimensions. At lower frequencies (in the high frequency regime) the wire current might be estimated with

$$I = \frac{-i\mu_0 v H_x^i \sin(k\nu)\dfrac{4e^{i\beta\Delta}}{\cos ka + \frac{\mu_0 v\sigma}{\beta}\sin ka}}{\gamma - \dfrac{\omega\mu_0}{2a}\displaystyle\sum_{n=1}^{\infty}\left\{\left[\sin\frac{n\pi}{2a}(\nu+a)\right]^2 \Big/ \sqrt{(\frac{\omega}{v})^2 - (\frac{n\pi}{2a})^2}\right\}} \qquad (1-16)$$

Equation 1-16 furnishes the wire current for an enclosure formed by two parallel plates of infinite extent (figure 5). A pulse given by equation 1-14 is incident normally on each plane. The planes are a distance 2a apart and the wire coordinate is ν_0 (figure 5).

Figure 5 also graphs the wire current for a parallel plate enclosure formed by plates 2 meters apart having the same conductivity and thickness as in the previous example. A similar wire is located 0.5 meters from one plane. The total field on the planes is one ampere/meter. The magnitude of the current is about the same as in the box example in figure 4 but the resonance spikes are more visible.

The code HFC has been written to treat the high frequency case with a great deal of precision. Figure 6 shows that it calculates correctly the scattering of an incident electromagnetic wave. The surface current density (amperes/meter) on the outside of the box is graphed around the perimeter of the box. Agreement is seen to be good with published results for the two frequencies discussed in section 6. The $k_a = 1$ case corresponds to a wavelength equal to three times the box dimension a.

The wire current can be computed as a function of time for the intermediate and high frequency cases by taking the inverse fourier transform

$$I(t) = \frac{1}{2\pi}\int_{-\infty}^{\infty} d\omega e^{-i\omega t} I(\omega)$$

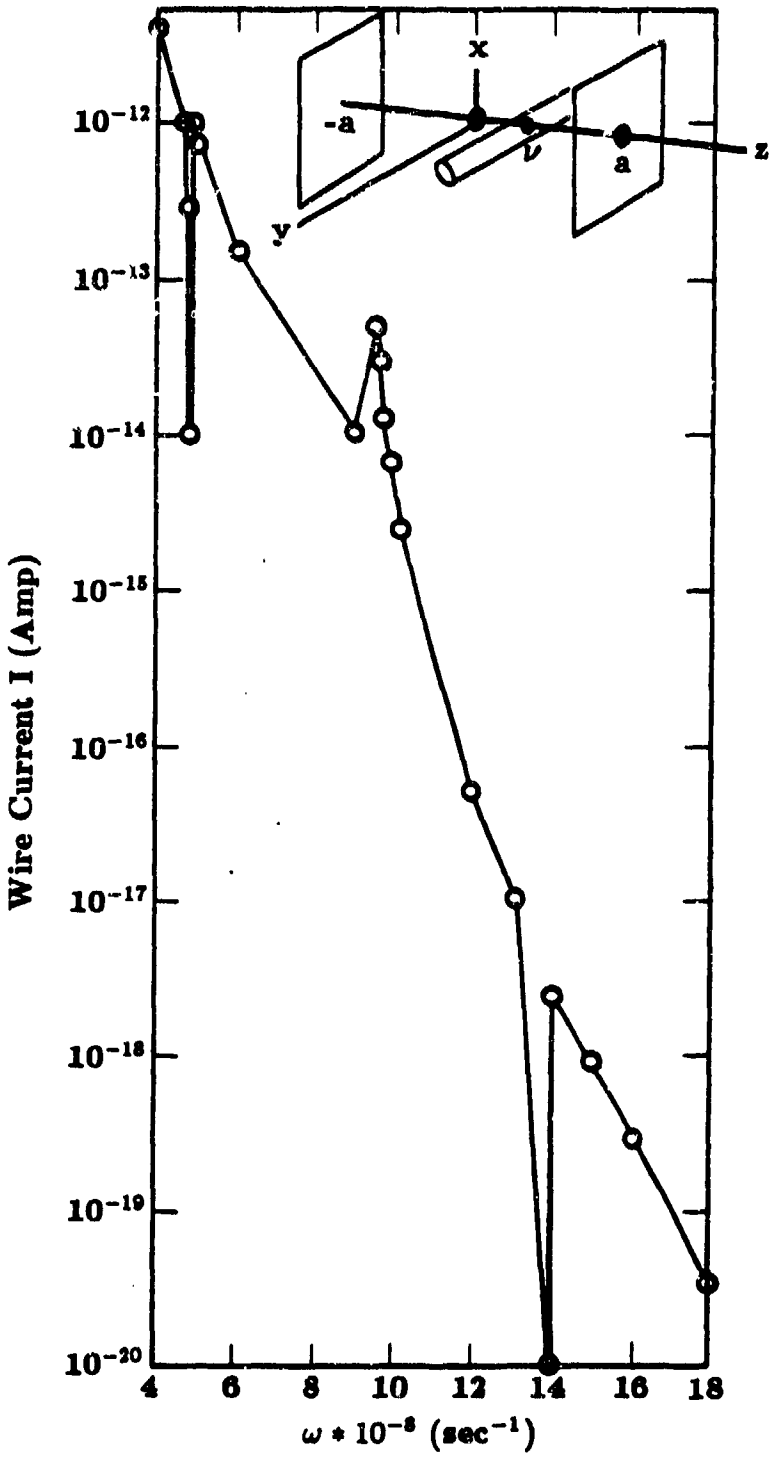

Figure 5. Parallel late wire current.

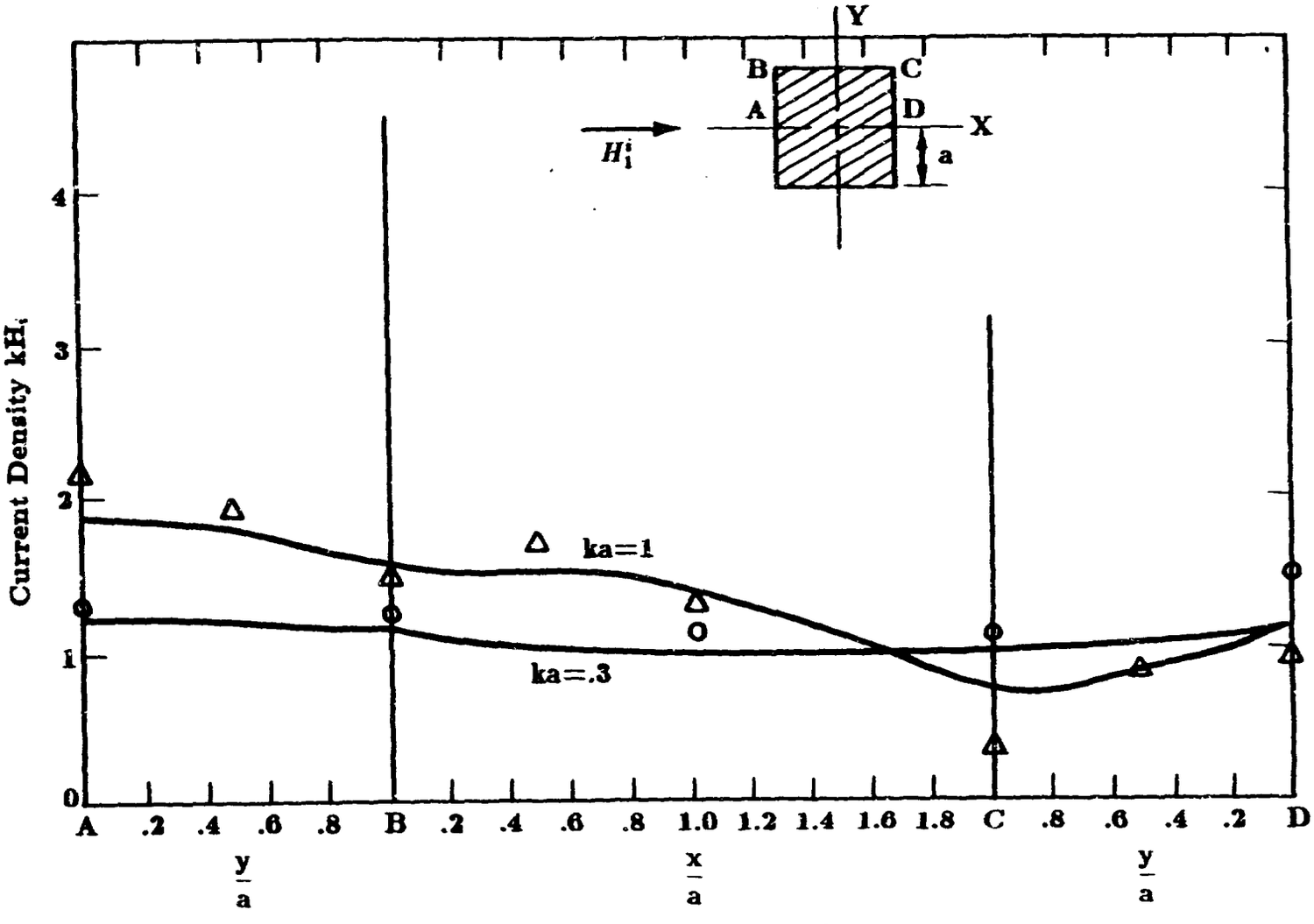

Figure 6. Surface current on a long square box in an H wave. The triangles correspond to ka = 1, circles to ka = .3. The solid lines are square cylinder calculations of Reference 8.

of equations 1-2, 1-13 or 1-16.

The parallel plate enclosure is discussed in section 3. Other high frequency results are explained in sections 4, 5 and 6.

1.5 Physics of Wire Current

The fundamental physics of the wire coupling is easily understood. The metallic conductor very effectively shields the incident electric field from the interior of the conductor at all frequencies. At low frequencies charge appears on the external surface (the conductor polarizes) which creates an electric field which cancels the incident field within the enclosure.

The incident magnetic field, however, slowly diffuses through the walls. The curl of the magnetic field creates a small electric field which drives current in the metal. The current creates its own magnetic field which cancels the incident field so that the internal magnetic field is small. This is the mechanism of inductive shielding which occurs in the low frequency regime. At higher frequencies the internal magnetic field is further reduced as the wave propagates many skin depths through the metal.

The dotted line in figure 7 defines a closed loop which runs through the wire and the metallic walls. Around this loop Faraday's law states

$$\mathrm{EMF} = \oint \mathrm{E} \cdot \mathrm{d}\ell = \mathrm{i}\omega\mu_0 \int \mathrm{H} \cdot \mathrm{ndS}$$

This equation indicates that the electromotive force driving current through the wire equals the rate of change of magnetic flux through the loop. Clearly, the magnetic flux increases as the magnetic field increases. The equation also predicts that as the frequency ω increases the EMF and wire current will increase. The rising portion of the wire current in figure 2 is due to this effect.

However, this source of EMF drives current against two types of impedance. Firstly, the frictional force exerted by the metallic lattice impedes the electrons flowing through it. This is quantified by the wire resistance. Secondly, the current flowing through the wire circuit creates a magnetic field which reduces the flux in the loop and, consequently, the EMF. This can be quantified in terms of the wire's self-inductance L. As

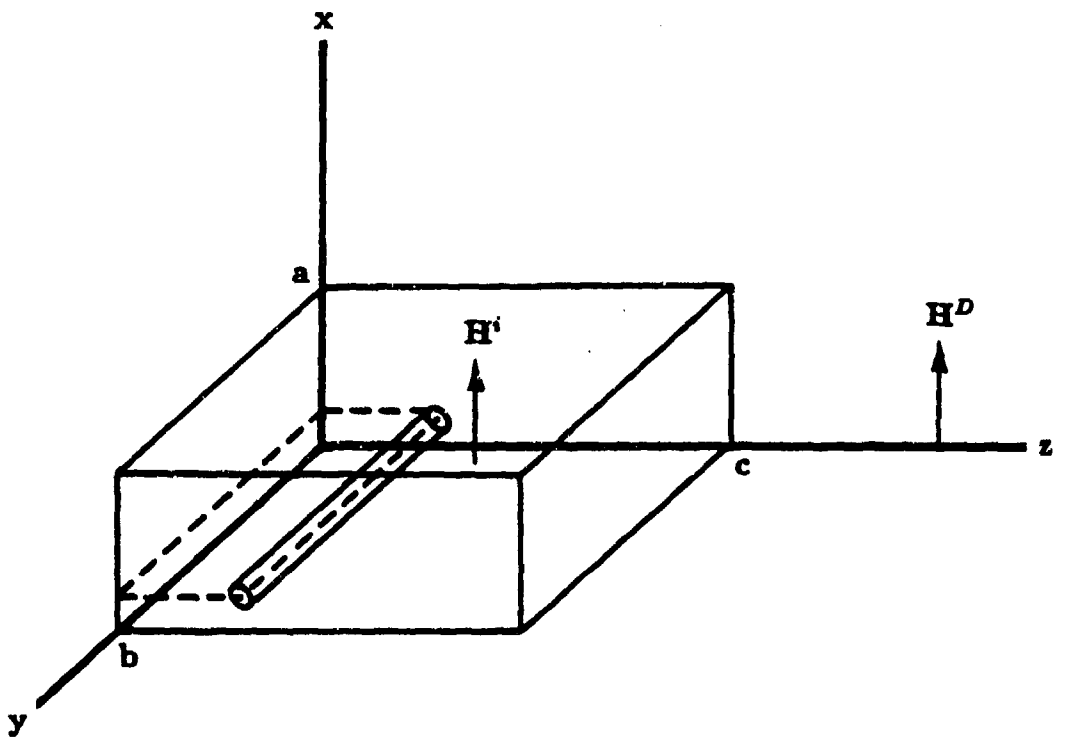

Figure 7. EMF in loop.

the frequency increases the inductive reactance increases and so the wire current decreases. This causes the drop in current in figure 2 at the higher frequencies.

In the low frequency regime the internal magnetic field is largely independent of the shape of the enclosure for reasons discussed in Appendix A and section 2. Furthermore, the inductance L is always of the order of μ_0 henry/meter regardless of whether the wire is straight or (within reason) curved. Consequently, the EMF in the loop in figure 7 and the wire current itself is expected to be somewhat insensitive to the precise shape of the enclosure or the wire.

The nature of the internal magnetic field in the low frequency inductive regime has been very well developed elsewhere[2,4,5] . If a short pulse is incident on an enclosure of any shape the internal magnetic field slowly rises from zero and reaches a peak after about $\tau_\Delta/4$ where

$$\tau_\Delta = \mu_0 \sigma \Delta^2 \quad \text{seconds} \quad .$$

Here Δ is the wall thickness. This is the time for the radiation to diffuse through the walls and is often tens of microseconds. The field then decays to zero exponentially with a fall time of

$$\tau_d = \xi \tau_\Delta$$

where ξ is the ratio of the volume of the enclosure to the volume of the walls. In general, then, if the incident pulse is shorter than τ_Δ then the internal magnetic field slowly rises to a peak after $\tau_\Delta/4$ seconds. It then falls even more slowly. The internal field behavior is totally insensitive to the detailed time history of the incident pulse. The internal electric field is induced b the changing internal magnetic field and, therefore, is proportional to the rate of change of the magnetic field.

The wire current can be expected to rise to a peak at about the time τ_D and then fall to zero. This behavior obtains as long as the pulsewidth is shorter than τ_Δ and is independent of the details of the incident pulse.

1.6 Mathematical Remarks

Several mathematical facts which will be used below are discussed in this section.

The electric and magnetic fields[3,6] can be written in terms of the vector A and scalar ϕ potentials

$$\mathbf{B} = \nabla \times \mathbf{A}$$

$$\mathbf{E} = -\nabla\phi - \frac{\partial \mathbf{A}}{\partial t} \quad . \tag{1-17}$$

In this report the Lorentz gauge is used exclusively.

Consider a scalar function ψ satisfying the differential equation

$$\nabla^2\psi - \frac{1}{v^2}\frac{\partial^2\psi}{\partial t^2} = 0 \quad . \tag{1-18}$$

Then, the transformation

$$\mathbf{A}_0 = \mathbf{A} - \nabla\psi$$

$$\phi_0 = \phi + \frac{\partial\psi}{\partial t}$$

yields new potentials which lead to the same E and B (equation 1-1) and satisfy the Lorentz gauge conditions. Although A and ψ must satisfy boundary conditions on the box, ψ can have any value on the boundaries (as well as any initial conditions) because the electric and magnetic fields on the boundary given by equation 1-1 are completely independent of ψ. Therefore, ψ can be any solution to the homogeneous wave equation (equation 1-2) which will be seen to be very useful.

The freedom afforded by ψ allows one to choose a scalar potential ϕ which is zero on the walls. For if ϕ were not zero on the walls then ψ could be chosen to have the value $\psi = \frac{\phi}{i\omega}$ on the walls. Then ψ must be that solution of the wave equation (equation 1-18) which has the prescribed value on the wall which is

$$\psi = \int \frac{\phi}{i\omega} \nabla G \cdot dS \quad . \qquad (1-19)$$

Here G is the Green's function of the wave equation satisfying Dirichlet boundary conditions and the integral is taken over the wall surfaces. Clearly, another scalar potential ϕ_0 could be defined

$$\phi_0 = \phi + \frac{\partial \psi}{\partial t} \quad . \qquad (1-20)$$

Of course, $\phi_0 = 0$ on the walls.

The Helmholtz equation

$$\nabla^2 \psi + k^2 \psi = -4\pi\rho$$

arises from fourier transform of the wave equation as well as the diffusion equation. It has the general solution[3]

$$\psi(\bar{r}) = \int \rho G dV + \frac{1}{4\pi} \int [G \nabla \psi - \psi \nabla G] \cdot dS$$

where the Green's function satisfies

$$\nabla^2 G + k^2 G = -4\pi\delta(\bar{r} - \bar{r}') \quad .$$

It is

$$G = 4\pi \sum_n \frac{\psi_n^*(\bar{r}')\psi_n(\bar{r})}{k_n^2 - k^2}$$

where ψ_n are eigenfunctions of the Helmholtz operator

$$\nabla^2 \psi_n + k^2 \psi_n = 0 \quad .$$

They are normalized according to

$$\int \psi_m^* \psi_n d\bar{r} = \delta_{mn}$$

ψ, G and ψ_n all satisfy the same boundary conditions.

SECTION 2

INTERMEDIATE FREQUENCY REGIME

2.1 Introduction

In the intermediate frequency regime the frequency is sufficiently high that the skin depth is smaller than the wall thickness but sufficiently low that the lowest mode of the box is not appreciably excited. For instance, if the wall conductivity and thickness are 10^6 mho/meter and one millimeter, respectively, and the box is 2 meters on a side then the intermediate frequency regime extends from about 1.6×10^6 to 2.5×10^8 sec^{-1}angular frequency.

At any point within the wire the current density J is related to the total electric field E_T by

$$J = \sigma_0 E_T \qquad (2-1)$$

where σ_0 is the wire conductivity. At low frequencies the current is uniform throughout the wire of radius w_0 so the total current is

$$I = \pi w_0^2 J \qquad (2-2)$$

and

$$IR_0 = E_T$$

where the wire resistance per unit length is

$$R_0 = \frac{1}{\pi w_0^2 \sigma_0} (\frac{\text{ohms}}{\text{m}}) \qquad (2-3)$$

At higher frequencies, however, the current runs primarily within a skin depth δ_0 of the wire surface and

$$IR_0(1-i)\frac{w_0}{2\delta_0} = E_T \quad . \qquad (2-4)$$

The total electric field is

$$E_T = E^e + E^w \quad . \qquad (2-5)$$

Here, E^e is the field within the box when the wire is not present but the box is irradiated with the external electromagnetic field. Similarly, E^w is the field within the box caused by a current I which runs down the wire and around the box when the external driving field is absent. Equations 2-4 and 2-5 indicate that the current on the wire must satisfy

$$IR_0(1-i)\frac{w_0}{2\delta_0} = E^e + E^w \qquad (2-6)$$

where the fields are evaluated at the wire. The derivation of this equation is very similar to the approach used in many scattering problems and is explained in greater detail in section A2 of Appendix A.

E^e and E^w are calculated in the following two subsections. Then equation 2-6 will be employed to calculate the current I in the wire.

2.2 Calculation of E^w

Figure 7 illustrates the problem geometry. A wire carrying a current density J connects opposite walls of a metallic box. The electric field within the box is sought. Of course, in order to drive the current there must be a source of electric field. For present purposes, however, it is only necessary to calculate the fields produced by the current so the details of this source are irrelevant.

The current in the wire can be written as a cosine series

$$J_y(x,y,z) = \sum_{p=1}^{\infty} J_p(x,z)\cos(\frac{p\pi y}{b}) \qquad (2-7)$$

where J_p is the fourier coefficient and is a function of the radial position. The time dependance is exp (-i ω t). The cosine series will faithfully converge to any possible wire current in the open interval (0,b) but at the wire ends the series fails. This causes no difficulty.

The Hertz Vector

It is helpful to employ the Hertz vector Π. The polarization vector P is defined in terms of the current density by

$$\frac{\partial \bar{P}}{\partial t} = J \qquad (2-8)$$

By the continuity equation, therefore, the charge density on the wire must be

$$\rho = -\nabla \cdot \bar{P} \quad . \qquad (2-9)$$

Maxwell's equations then become

$$\nabla \times H = \frac{\partial P}{\partial t} + \frac{\partial D}{\partial t} \qquad \nabla \cdot E = -\frac{1}{\epsilon_0}\nabla \cdot P$$

$$\nabla \cdot B = 0 \qquad \nabla \times E = -\frac{\partial B}{\partial t} \qquad (2-10)$$

It is easily shown that these are satisfied by the electric and magnetic fields given by

$$\bar{E} = \nabla(\nabla \cdot \bar{\Pi}) - \frac{1}{v^2}\frac{\partial^2 \bar{\Pi}}{\partial t^2}$$

$$\bar{B} = \frac{1}{v^2}\nabla \times \frac{\partial \bar{\Pi}}{\partial t} \qquad (2-11)$$

where the Hertz vector satisfies

$$\nabla^2\vec{\Pi} - \frac{1}{v^2}\frac{\partial^2\vec{\Pi}}{\partial t^2} = -\frac{1}{\epsilon_2}\vec{P} \qquad (2-12)$$

The speed of light in vacuum is called v since c denotes the box length.

In terms of the vector and scalar potential (section A)

$$E = -\frac{\partial A}{\partial t} - \nabla\phi \qquad (2-13)$$

$$B = \nabla \times A \quad . \qquad (2-14)$$

Comparing equations 2-11 and 2-13 and 2-14 shows how Π depends upon A and ϕ

$$A = \frac{1}{v^2}\frac{\partial \Pi}{\partial t}$$

$$\phi = -\nabla \cdot \Pi \qquad (2\text{-}15)$$

Boundary Conditions

Since the wall conductivity is finite the inside and outside of the box are coupled. An exact solution would solve for the exterior and interior fields together. Because the skin depth in the intermediate region is small, however, the coupling is extremely small and the exterior fields are minuscule compared to those in the interior. Consequently, the walls will be approximated as perfect conductors to calculate E^w.

The Hertz vector has three components but only the Π_y component is non-zero. This appears reasonable since P has only a y-component so that only Π_y is driven through equation 2-12. But this is insufficient to prove that Π_x and Π_z are non-zero because the homogeneous equation has non-zero solutions. Instead, the assumption that Π_x and Π_z are zero can be justified at the end of the calculation by verifying that the final solution satisfies Maxwell's equations. It has been pointed out in section A that it is always possible to choose a scalar potential ϕ such that on the walls

$$\phi = 0 \quad . \tag{2-16}$$

On the x=0 and x=a and z=0 and z=c walls, $E_y = 0$. From equation 2-11 and equation 2-15 on the walls

$$\nabla \cdot \Pi = 0 \tag{2-17}$$

and

$$E_y = \frac{\partial}{\partial y}(\nabla \cdot \Pi) + \frac{\omega^2}{v^2}\Pi \quad , \tag{2-18}$$

so that on these walls

$$\Pi = 0 \quad . \tag{2-19}$$

On the y=0 and y=b walls equation 2-15 shows

$$\nabla \cdot \Pi = 0$$

so that

$$\frac{\partial \Pi}{\partial y} = 0 \tag{2-20}$$

Equations 2-19 and 2-20 are the boundary conditions on Π.

Therefore, by the remarks in the last subsection of section 1 the Hertz potential is

$$\Pi_y = \frac{1}{4\pi\epsilon_0}\int P_y G dV \tag{2-21}$$

where G is the Green's function

$$G = 4\pi \frac{8}{abc} \sum_{\substack{\ell,n=1 \\ m=0}}^{\infty} \frac{\sin\frac{\ell\pi x}{a}\cos\frac{m\pi y}{b}\sin\frac{n\pi z}{c}\sin\frac{\ell\pi x'}{a}\cos\frac{m\pi y'}{b}\sin\frac{n\pi z'}{c}}{(k_n^2 - k^2)} \left(\frac{1}{2}\right)^{\delta_{m0}} \qquad (2-22)$$

where

$$k_n^2 = (\frac{\ell\pi}{a})^2 + (\frac{m\pi}{b})^2 + (\frac{n\pi}{c})^2$$

and $k = \omega/c$. The exponent δ_{m0} is one if m=0 and zero otherwise. Here G satisfies Dirichlet boundary conditions on two walls and Neumann conditions on the other. Of course the current runs primarily within a skin depth of the surface of the wire but the analysis is simplified by approximating the current to run along a very thin filament so that

$$J_y = \sum_{p=1}^{\infty} I_p \delta(x-\xi)\delta(z-\eta)\cos(\frac{p\pi y}{b}) \quad . \qquad (2-23)$$

From equation 2-8 the polarization P_y is found and the Hertz vector is

$$\Pi_y = \frac{-4}{i\omega ac\epsilon_o} \sum_{\substack{\ell,n=1 \\ m=0}}^{\infty} I_m \frac{\sin(\frac{\ell\pi x}{a})\cos(\frac{m\pi y}{b})\sin(\frac{n\pi z}{c})\sin(\frac{\ell\pi\xi}{a})\sin(\frac{n\pi\eta}{c})}{k_n^2 - k^2} \qquad (2-24)$$

From equation 2-11 the electric field within the cavity can be computed. At the wire location it is

$$E^w(y) = \frac{-4}{i\omega ac\epsilon_0} \sum_{\substack{\ell,n=1 \\ m=0}}^{\infty} \left\{ I_m \frac{[\frac{\omega^2}{v^2} - (\frac{m\pi}{b})^2]}{k_n^2 - k^2} \sin^2\frac{\ell\pi\xi}{a}\sin^2\frac{n\pi\eta}{c} \right\} \cos\frac{m\pi y}{b} \quad . \qquad (2-25)$$

This is the desired field at the wire which will be needed below.

The advantage of the Hertz vector approach is that it simplifies the boundary conditions. The boundary condition which was employed is that the electric field tangent to the walls is zero while the derivative of the normal electric field is zero (since the divergence of the electric field is zero just inside the wall where the tangential electric field vanishes). But the electric field is due to the combined affect of both A and ϕ. Hence, the boundary condition mixes the behavior of A and ϕ. The Hertz vector provides one approach to unmix the boundary conditions. Another possible approach is to solve the scalar retarded potential equation subject to the conditions that ϕ is zero on the walls. With this value of ϕ the boundary condition for A can be found from

$$\frac{\partial \mathbf{A}}{\partial t} = -\mathbf{E} - \nabla\phi \quad .$$

2.3 External Driver E^e

In this section the electric field E^e produced within the enclosure is calculated when the wire is not present. In sections 4 and 5 this problem is solved with the help of the code HFC very precisely for the high frequency regime. This numerical method is applicable to the intermediate frequency case also and will yield a very accurate solution. However, in the intermediate frequency regime the code treatment is unnecessarily complicated. The method developed in this section is expected to yield a simple, accurate result.

Figure 8 illustrates three enclosures which are irradiated by an electromagnetic wave whose wavelength in free space is much smaller than the enclosure. Since the wavelength is large the external magnetic field is constant around the enclosure (Appendix A) and is given by

$$H^D e^{-i\omega t} \quad . \qquad (2-26)$$

The internal field H^i is constant in each case and points in the direction of the external field. For the sphere, parallel plates, and two polarizations of the cylinder[2,5]

$$H^i = H^D \left\{ \cos(\beta\Delta) - \frac{\beta\bar{a}}{3}\sin(\beta\Delta) \right\}^{-1} \qquad (2\text{-}27)$$

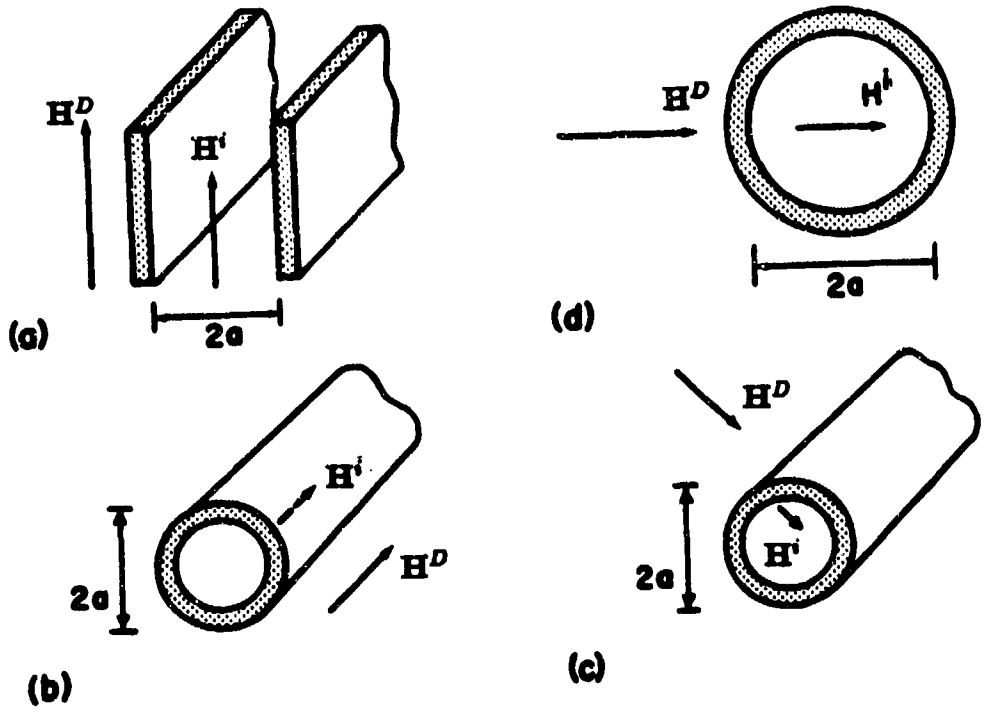

Figure 8. (a) Two parallel plates, (b) a cylindrical shell with longitudinal H^D, (c) a cylindrical shell with transverse H^D, and (d) a spherical shell. All cavity walls have thickness Δ, conductivity σ (taken from EMF Interaction: K. S. Lee, AFWL-TR-80-402).

$$H^i = H^D \{\cos(\beta\Delta) - \beta\bar{a}\sin(\beta\Delta)\}^{-1} \tag{2-28}$$

$$H^i = H^D \left\{\cos(\beta\Delta) - \frac{\beta\bar{a}}{2}\sin(\beta\Delta)\right\}^{-1} \tag{2-29}$$

where $\beta^2 = 1\omega\mu_0\sigma$ ($\beta = (1+i)/\delta$ where δ is the skin depth). The dimension $\bar{a}$ is defined in the figure and Δ is the wall thickness. Clearly, the internal field is almost the same regardless of the geometry. It is reasonable to assume, therefore, that the field within a box is also approximately uniform and its magnitude is roughly that of a spherical enclosure. If the sides of the box are equal the box might best be replaced by a sphere whereas if one side of the box is very small it would best resemble two parallel plates. Fortunately, the above formulas indicate that all geometries have about the same internal fields.

Equation 2-27, therefore, will be used to approximate the uniform field within the box. The sphere's radius is chosen to be

$$\bar{a} = \left(\frac{3abc}{4\pi}\right)^{1/3} \tag{2-30}$$

so that the volume of the sphere and box are the same. In Appendix A the field within a box and sphere are shown to be nearly the same in the low frequency regime by numerically solving for the internal field with the code BOX4.

Equation 2-27 is derived in the remainder of this subsection. In section 2 of Appendix A it is shown that the magnetic field within an enclosure is governed by the static magnetic field equations whenever the enclosure is driven at a frequency much less than the lowest modal frequency of the box. Consequently the internal (and external) magnetic field are given by the gradient of a magnetic potential which satisfies Laplace's equation. Assuming that the form of the potentials are (c.f. figure 9)

$$\begin{aligned} \Omega^{in} &= H^i r\cos\theta \\ \Omega^{out} &= H^D r\cos + \frac{B_1}{r^2}\cos\theta \end{aligned} \tag{2-31}$$

the fields tangential to the sphere are

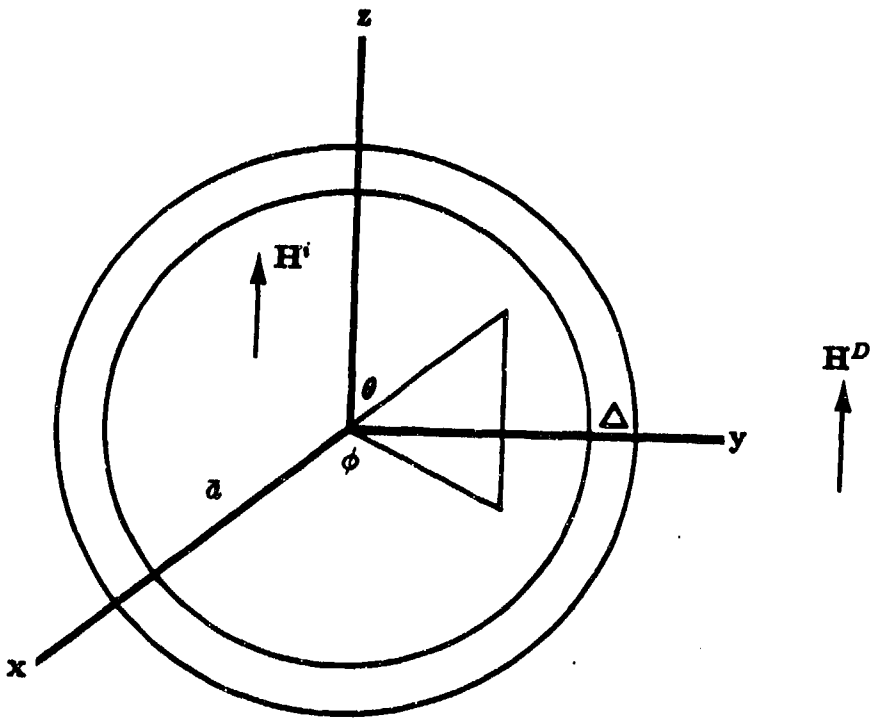

Figure 9. Spherical enclosure.

$$H_4 = -H^i \sin\theta$$

$$H_1 = -H^D \sin\theta - \frac{B_1}{a^3}\sin\theta \quad . \tag{2-32}$$

Within the conductor

$$\nabla^2 H + \beta^2 H = 0 \tag{2-33}$$

which can be solved by separation of variables to be the product of spherical Hankel functions and $\sin\theta$. In the limit that the skin depth is smaller than the spheres radius the two independent solutions are

$$\frac{-H_2}{\beta r} e^{i\beta r}\sin(\theta) \quad \text{and} \quad -\frac{H_3}{\beta r} e^{i\beta r}\sin(\theta) \tag{2-34}$$

The electric field associated with each magnetic field is given by

$$E = \frac{1}{\sigma}\nabla \times H \tag{2-35}$$

so that the two independent solutions of electric field are

$$\frac{-iH_2}{\sigma r} e^{i\beta r}\sin(\theta) \quad \text{and} \quad \frac{iH_3}{\sigma r} e^{-i\beta r}\sin(\theta) \tag{2-36}$$

The continuity of the magnetic and electric field across the sphere's inner surface yields

$$-H^i = -\frac{H_2}{\beta \bar{a}} e^{i\beta \bar{a}} + \frac{H_3}{\beta \bar{a}} e^{i\beta \bar{a}} \tag{2-37}$$

$$i\omega\mu_0 \frac{\bar{a}}{2} H^i = \frac{-iH_2}{\sigma \bar{a}} e^{i\beta \bar{a}} + \frac{iH_3}{\sigma \bar{a}} e^{-i\beta \bar{a}} \tag{2-38}$$

whereas the continuity of the magnetic field across the outer surface provides

$$-H^D - \frac{\beta_1}{\bar{a}^3} = -\frac{H_2}{\beta b}e^{i\beta b} - \frac{H_3}{\beta b}e^{-i\beta b} \qquad (2-39)$$

Within the conductor the normal component of the magnetic field satisfies Faraday's law. At the outer surface it equals the normal component of the external magnetic field. Consequently,

$$(\nabla \times E)_n = i\omega\mu_0 H_n = i\omega\mu_0 \frac{\partial \Omega^{out}}{\partial r} \qquad (2-40)$$

and from equations 2-31 and 2-36

$$\frac{1}{\bar{a}\sin\theta}\frac{\partial}{\partial\theta}\sin^2\theta\left\{\frac{-iH_2}{\sigma\bar{a}}e^{i\beta a} + \frac{iH_3}{\sigma\bar{a}}e^{-i\beta a}\right\} = i\omega\mu_0\left\{H_{ex} - \frac{2B_1}{\bar{a}^3}\right\}\cos\theta \qquad (2-41)$$

Solving simultaneously equations 2-37, 2-38, 2-39, 2-41 yields equation 2-27. As expected, in the limit that the skin depth is larger than the wall thickness the low frequency internal magnetic field employed in equation 1-2 of Appendix A is obtained.

Following the low frequency treatment in Appendix A (equation A-12) the average field in the walls is

$$\mu_0\frac{bc}{2(b+c)}i\omega H \qquad (2-42)$$

and the electric field at the wire which runs in the y-direction (figure 7) with the coordinates $x = \xi$ and $z = \eta$ is

$$E^e = -\frac{\partial A_y}{\partial t} = \mu_0\left(\eta - \frac{c}{2}\right)\frac{H^D}{\cos(\beta\Delta) - \frac{\beta a}{s}\sin(\beta\Delta)}\frac{b}{b+c} \quad . \qquad (2-43)$$

2.4 Intermediate Frequency Result

The wire current follows from substituting E^w and E^e from equations 2-25 and 2-43 in equation 2-6. Because the electric field E^e created by the external electromagnetic pulse is uniform along the wire it drives a uniform current down the wire and, consequently, only the m = 0 mode in equation 2-25 is retained. The wire current is, therefore,

$$I = \frac{i\omega\mu_0 H^D(\eta - \frac{c}{2})\dfrac{1}{\cos(\beta\Delta) - \frac{1}{2}\beta\bar{a}\sin(\beta\Delta)}\dfrac{b}{b+c}}{\dfrac{(1-i)}{2\pi w_0\delta_0\sigma_0} - i\dfrac{8\omega\mu_0}{ac\pi^2}\displaystyle\sum_{\ell,n=1}^{\infty}\dfrac{\sin^2(\frac{\ell\pi\xi}{a})\sin^2(\frac{n\pi\eta}{c})}{(\frac{\ell}{a})^2 + (\frac{n}{c})^2}} \quad . \qquad (2-44)$$

Clearly, the real and imaginary parts of the denominator can be considered to be the resistive and inductive parts of the wire impedance within the box.

The only significant approximation made in the derivation has been to approximate the internal field by the field of a sphere. Appendix A indicates that this is a very good approximation in the small number of cases which are treated. Perhaps the most convincing argument that the approximation is always valid lies in figure 8 which suggests that the internal field is insensitive to the enclosure geometry.

SECTION 3

HIGH FREQUENCY-PARALLEL PLATE ENCLOSURE

3.1 Introduction

At very high frequencies not only is the skin depth smaller than the wall thickness but the electromagnetic modes of the enclosure are excited. Consequently, the internal magnetic field can no longer be expected to be constant. In sections 4 and 5 the problem is treated precisely but the formal solution is complex and somewhat inconvenient to use. In this section the physics of the high frequency regime is examined by calculating the current excited on a wire within the enclosure formed by two infinite parallel conductors (figure 10). The simplified geometry allows an exact solution to be derived.

3.2 Parallel Plate Enclosure

Figure 10 illustrates an enclosure formed by two parallel conducting plates. On the external surface of both plates is an oscillating electric and magnetic field

$$H_x = H_1 e^{-i\omega t}$$

$$E_y = E_1 e^{-i\omega t} \tag{3-1}$$

as illustrated. These fields might be produced, for instance, if each plate were exposed to a plane electromagnetic wave. The fields H_1 and E_1 are the sum of the incident and reflected wave. Again the wire current must satisfy equation 2-6 and it is only necessary to calculate E^w and E^s.

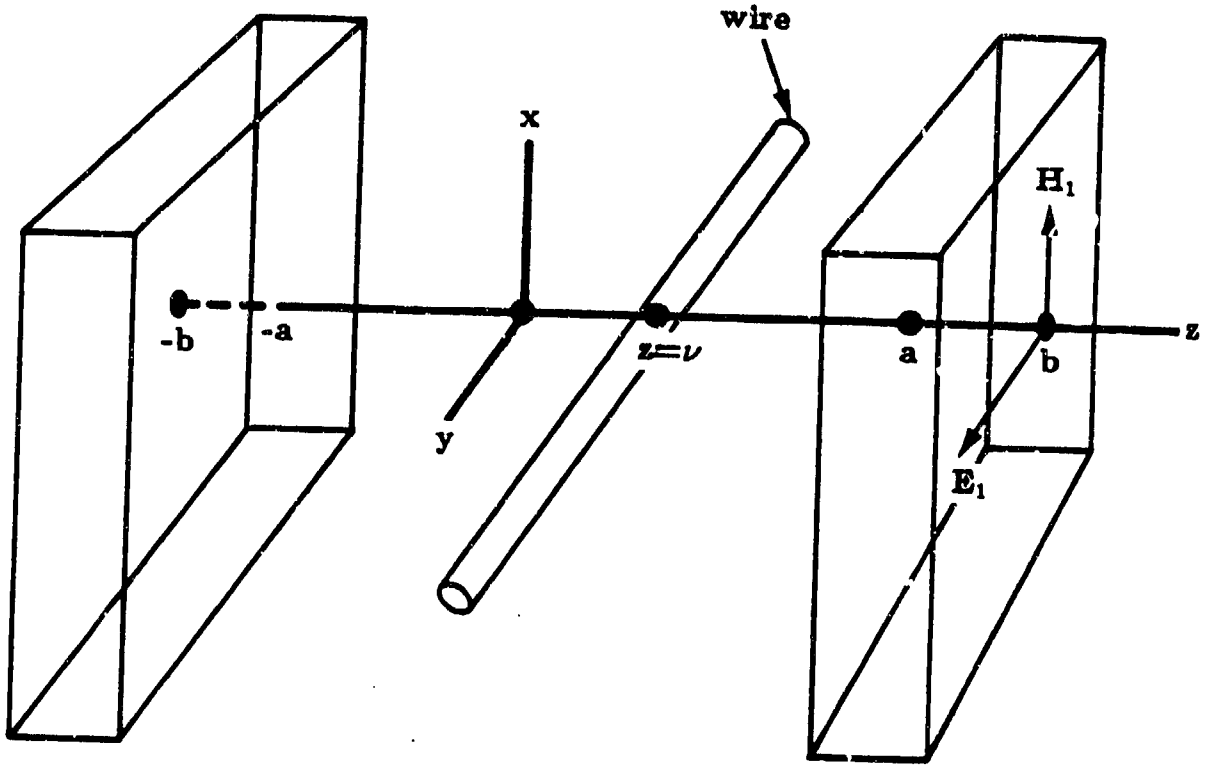

Figure 10. Parallel plate enclosure.

Calculation of E^s

If the wire is absent then the electric and magnetic fields within the enclosure satisfy the free space wave equations. Because the cavity excitation is identical on both plates the internal magnetic field is symmetrical about z = 0. Hence, the internal field is

$$H^i = H_4 \cos(kz) e^{-i\omega t} \qquad (3-2)$$

where $k = \omega/v$. The internal electric field can be found by Ampere's law

$$E_y = -\frac{1}{i\omega\epsilon_0}\frac{\partial H}{\partial z} \qquad (3-3)$$

to be

$$E_y = \frac{1}{i\epsilon_0 v} H_4 \sin(kz) e^{-i\omega t} \quad . \qquad (3-4)$$

Within the conductor the two independent solutions of the wave equation are

$$H_2 e^{i\beta z}$$

and

$$H_3 e^{-i\beta z} \qquad (3-5)$$

and the electric field of these modes

$$\frac{i\beta}{\sigma} H_2 e^{i\beta z}$$

and

$$\frac{-i\beta}{\sigma} H_3 e^{-i\beta z} \qquad (3-6)$$

can be calculated from Faraday's law.

Equating the tangential components of E and H at z=a and the tangential components of H at z=b yield three algebraic equations which can be solved for the unknowns H_2, H_3 and H_4. Solving yields the internal magnetic field in terms of the external

$$H_4 = \frac{H_1}{\cos(ka)\cos(\beta\Delta) - \frac{i\sigma}{\epsilon_0 v\beta}\sin(ka)\sin(\beta\Delta)} \qquad (3-7)$$

From equation 3-4 the internal electric field is

$$E_y = \frac{-i\mu_0 v H_1 \sin(kz)e^{-i\omega t}}{\cos(ka)\cos(\beta\Delta) - \frac{i\sigma}{\epsilon_0 v\beta}\sin(ka)\sin(\beta\Delta)} \qquad (3-8)$$

As expected, equation 3-7 reduces to equation 2-28 in the limit that the frequency is so low that $ka \ll 1$. Comparing these expressions indicates that the high frequency modal structure of the enclosure enters only through the sin and cosine of the argument ka.

3.3 Calculation of Wire Driver E^w

The coordinate system in figure 11 is employed to calculate E^w the field produced by the wire if the external driving wave is absent. The parallel walls are again approximated as perfect conductors which is an excellent assumption at high frequency when the walls are good shields. The walls are located at $z = 0$ and $z = 2a$ and the wire runs parallel to the y axis and is located at $x = 0$ and $z = \xi$.

The case is treated in which the wire current and electric field are independent of the y- coordinate. The y- component of the electric field obeys the wave equation

$$\frac{\partial^2 E}{\partial x^2} + \frac{\partial^2 E}{\partial z^2} + \frac{\omega^2}{v^2}E = -i\omega\mu_0 J \qquad (3-9)$$

subject to the boundary condition that it vanishes at the walls. This equation will be transformed by the fourier sine series

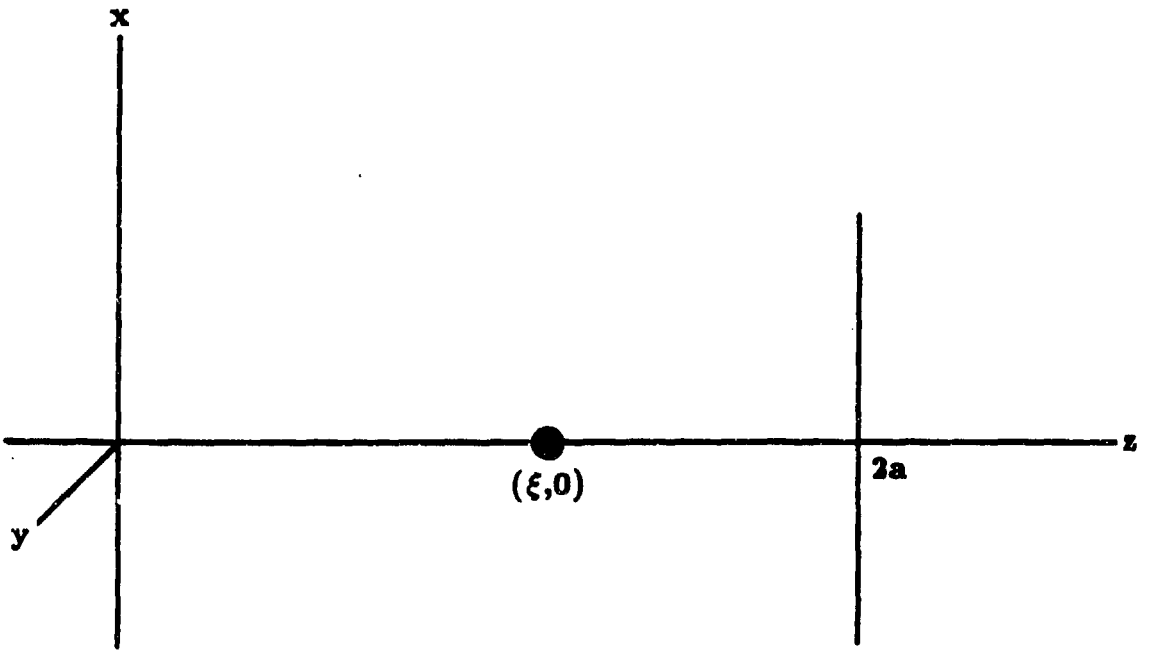

Figure 11. Parallel plate enclosure.

$$E_n(x) = \frac{1}{a}\int_0^{2a} E(x,z)\sin\frac{n\pi z}{2a}dz$$

$$E(x,z) = \sum_{n=1} E_n(x)\sin\frac{n\pi z}{2a} \qquad (3\text{-}10)$$

in the z variable and fourier transformed in the x variable by

$$E_n(k) = \frac{1}{2\pi}\int E_n(x)e^{-ikx}dx$$

$$E_n(x) = \int E_n(k)e^{ikx}dk \qquad (3\text{-}11)$$

Then the transformed electric field is

$$E_n(k) = \frac{i\omega\mu_0 J_n(k)}{k^2 + (\frac{n\pi}{2a})^2 - (\frac{\omega}{v})^2} \qquad (3-12)$$

where $J_n(k)$ is the transformed wire current density J. The convolution theorem indicates

$$E_n(x) = \frac{1}{2\pi}\int dx J_n(x) f(x-x') \qquad (3-13)$$

where

$$f(x) = \int dk e^{ikx}\frac{i\omega\mu_0}{(k-\alpha)(k+\alpha)} \qquad (3-14)$$

and

$$\alpha = \sqrt{(\frac{\omega}{v})^2 - (\frac{n\pi}{2a})^2} \quad . \qquad (3-15)$$

It is assumed that the field damps very slightly due to an unspecified mechanism. Then ω must have a small, negative imaginary part since the temporal dependance is exp (-i ω t). The poles are at α and -α. The square root appearing in the definition of α is chosen to be that branch of the function for which if

$$u = |u| e^{i\theta} \qquad -\pi < \theta < \pi$$

then

$$\sqrt{u} = \sqrt{|u|} e^{i\theta/2} \quad . \tag{3-16}$$

Figure 12 shows ω/v with its small imaginary part. Also indicated is the value of α for several values of the integer n. The corresponding values of -α are shown. The inverse transform is done by closing the contour in the upper k plane when x is greater than zero. Yielding

$$f(x) = \frac{\pi\omega\mu_0 e^{-ix\sqrt{(\frac{\omega}{v})^2 - (\frac{n\pi}{2a})^2}}}{\sqrt{(\frac{\omega}{v})^2 - (\frac{n\pi}{2a})^2}} \quad .$$

Finally, the inverse sine series is inverted to yield the desired value of E^w

$$E^w(x,z) = \frac{\omega\mu_0 I}{2a} \sum_{n=1} \sin(\frac{n\pi\xi}{2a}) \frac{e^{-ix\sqrt{(\frac{\omega}{v})^2 - (\frac{n\pi}{2a})^2}}}{\sqrt{(\frac{\omega}{v})^2 - (\frac{n\pi}{2a})^2}} \sin(\frac{n\pi z}{2a}) \tag{3-17}$$

The field at the wire is found by evaluating this expression at x = 0 and z = ξ. It is assumed that the wire current density is J = I $\delta(z - \xi)\delta(x)$.

3.4 Wire Current in Parallel Plate Enclosure

The wire current is found to be

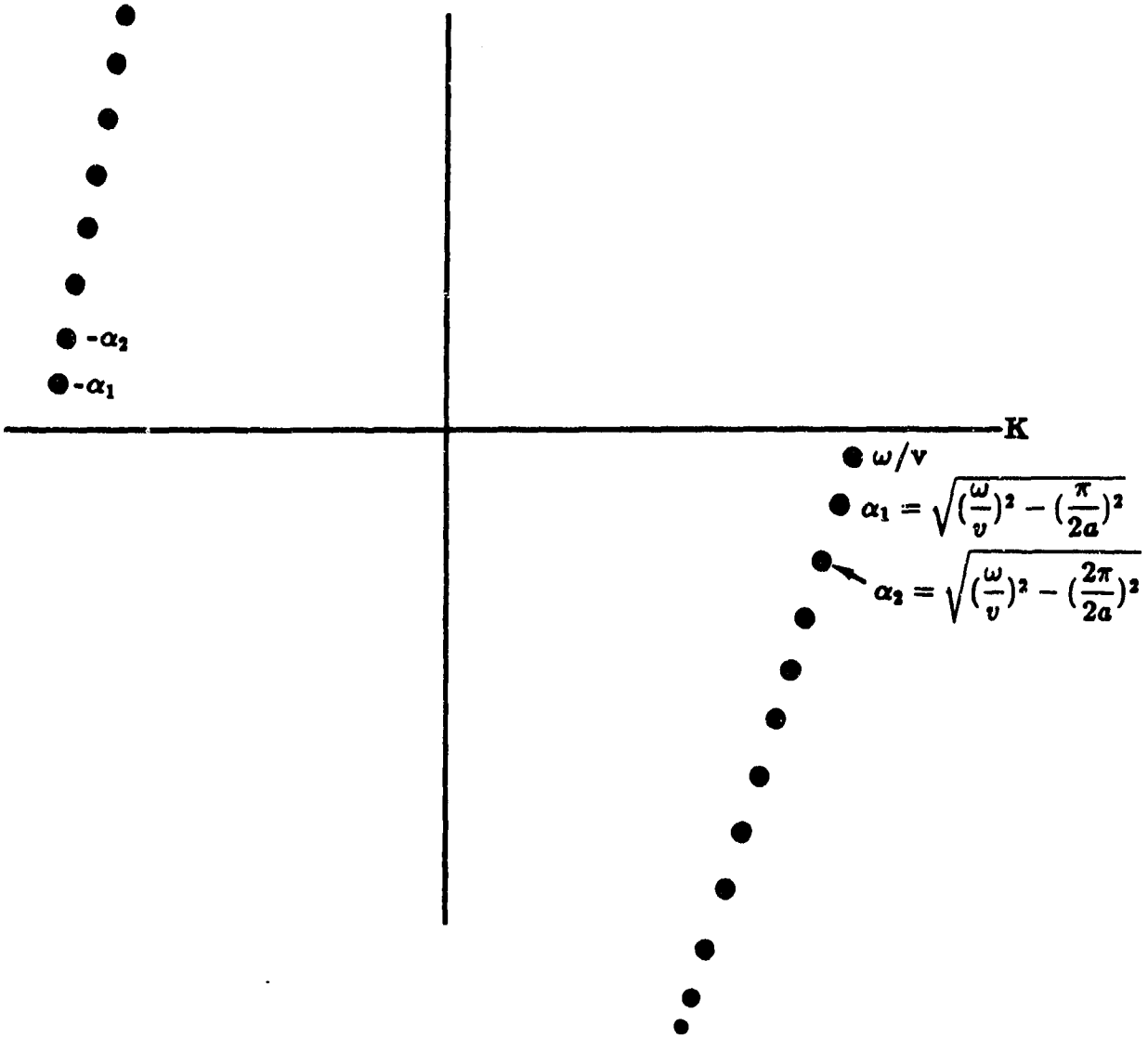

Figure 12. Complex K plane.

$$I = \frac{-i\mu_0 v H_1 \sin(k\nu)\dfrac{2e^{i\beta\Delta}}{\cos ka + \frac{\mu_0 v\sigma}{\beta}\sin ka}}{\frac{(1-i)}{2\pi w_0 \sigma_0 \delta_0} - \frac{\omega\mu_0}{2a}\sum_{n=1}\left\{\left[\sin\frac{n\pi}{2a}(\nu+a)\right]^2 / \sqrt{\left(\frac{\omega}{v}\right)^2 - \left(\frac{n\pi}{2a}\right)^2}\right\}} \qquad (3-18)$$

by substituting equations 3-8 and 3-17 in equation 2-6. By definition $\beta\Delta$ in the high frequency regime is large so the large argument limits of the sin and cosine functions have been employed. Furthermore, equation 3-17 has been adjusted to conform to the figure 10 coordinate system by evaluating the wire location at $\nu = \xi + a$.

At first glance it might be thought that the wire current would be very large if the incident wave frequency equals the frequency of one of the modes of the cavity. This analysis indicates that the wire current is large but not huge at the modal frequencies. The electric field induced within the cavity is largest when the expression (equation 3-18)

$$\cos(ka) + \frac{\mu_0 v\sigma}{\beta}\sin(ka) \qquad (3-19)$$

is smallest. For practical values of the conductivity the minimum value is one which occurs when sin ka = 0. As expected the minimum occurs whenever the driving frequency equals the frequency of one of the internal modes of the cavity (if its wall conductivity were infinite). But β is a complex number. Hence, there is no real value of $k = \omega/v$ for which equation 3-19 vanishes. Therefore the internal field is finite. Evidently, if the walls are made of metal then the conductivity always introduces enough damping to prevent the internal field from becoming very large. If the walls were made of a very poor conductor, however, then equation 3-18 shows that the internal field could be driven to large values. The upward spikes in figure 5 illustrate the increased current.

The square root in equation 3-18 is also zero whenever the driving frequency equals the frequency of an internal mode. This causes the wire current to be zero which is not surprising for at for these frequencies a finite wire current causes an infinite electric field. If the finite wall conductivity were taken into account then the current would be small but not zero. Consequently, equation 3-18 indicates that the wire current at these frequencies is zero which is an underestimate. The downward spikes in figure 5 illustrates this behavior.

The internal field is driven maximally whenever $ka = n\pi$ or

$$\frac{\omega a}{v} = n\pi \qquad (3-20)$$

whereas the square root is zero if

$$\frac{\omega a}{v} = \frac{1}{2}m\pi \quad . \qquad (3-21)$$

The difference is attributable to the fact that the external field is assumed to be equal on each conducting plate. Hence, it can excite only modes of E^e which are anti-symmetric in z. The wire, however, excites both symmetric and anti-symmetric modes depending on its location. It should be pointed out that the peak current at each upward spike is also underestimated because whenever equation 3-20 is satisfied equation 3-21 is satisfied also for $m = 2n$.

SECTION 4

HIGH FREQUENCY REGIME - APPROXIMATE TREATMENT

In the low and intermediate frequency regime the electromagnetic field within the enclosure is approximately uniform and easily calculated with equation 2-27 and 2-43 of section 2. At high frequencies, however, the internal field depends upon the frequency and angle of incidence of the incident electromagnetic wave which greatly complicates the problem of predicting the wire current. Several approximations are made in this section in order to derive an easily applied formula to estimate the wire current. In section 5 a more exact treatment is derived.

4.1 Inductance Matrix

In this section electromagnetic transmission through a conducting plane is examined in some detail. Figure 13 illustrates a conductor of thickness Δ which is irradiated normally from the right with a linearly polarized, plane electromagnetic wave of frequency ω. The total field at $z = \Delta$ is the sum of the incident and reflected waves and is denoted by E^1 and H^1. Similarly, the total field at the $z = 0$ plane is E^4 and H^4.

Within the conducting medium two independent solutions to the diffusion equation exist. The total internal magnetic fields is

$$H(z,t) = H_2 e^{i\beta z} + H_3 e^{-i\beta z} \qquad (4-1)$$

The total electric field is derived from Faradays law to be

$$E(z,t) = \frac{i\beta}{\sigma} H_2 e^{i\beta z} - \frac{i\beta}{\sigma} H_3 e^{-i\beta z} \qquad (4-2)$$

The wave H^2 travels to the right while H^3 travels to the left.

The electric and magnetic fields are continuous across the surface. Equating the internal and external fields at the two surfaces leads to four algebraic equations which

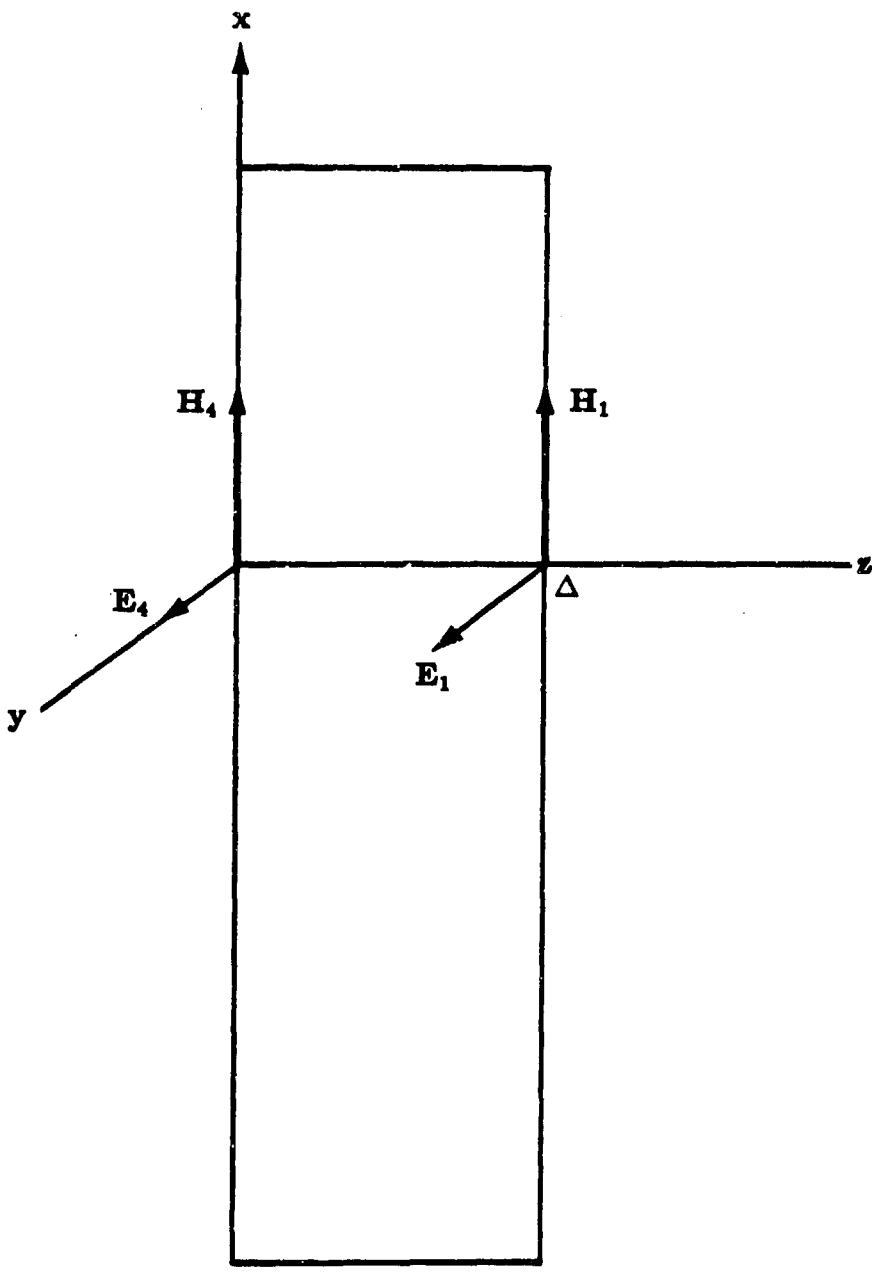

Figure 13. Metallic slab.

contain the six quantities H^1 through H^4 and E^1 and E^4. It is useful to consider H^1 and H^4 to be known and solve for the remaining quantities in terms of them. Then

$$\begin{aligned} E_1 &= Z_s H_1 - Z_t H_4 \\ E_4 &= Z_t H_1 - Z_s H_4 \end{aligned} \tag{4-3}$$

where

$$\begin{aligned} Z_s &= \frac{\beta}{\sigma} \frac{\cos \beta \Delta}{\sin \beta \Delta} \\ Z_t &= \frac{\beta}{\sigma \sin \beta \Delta} \end{aligned} \tag{4-4}$$

are the self impedance and transfer impedance. This can be written in matrix form as

$$\begin{bmatrix} E_1 \\ E_4 \end{bmatrix} = \begin{bmatrix} Z_s & -Z_t \\ Z_t & -Z_s \end{bmatrix} \begin{bmatrix} H_1 \\ H_4 \end{bmatrix} . \tag{4-5}$$

In terms of the fields on the $z = \Delta$ surface, H^1 and E^1, the magnetic field phasors in the metal are

$$\begin{aligned} H_2 &= \frac{1}{2} H_1 e^{-i\beta\Delta} + \frac{1}{2} \frac{\sigma}{i\beta} e^{-i\beta\Delta} E_1 \\ H_3 &= \frac{1}{2} H_1 e^{i\beta\Delta} - \frac{1}{2} \frac{\sigma}{i\beta} e^{i\beta\Delta} E_1 \end{aligned} . \tag{4-6}$$

The electromagnetics are explained in figure 14 assuming that the driving wave is incident at the $z = \Delta$ surface. On the $z = 0$ surface the ratio of electric and magnetic fields within the conductor is constrained to be equal to the impedance Z_s of the electromagnetic

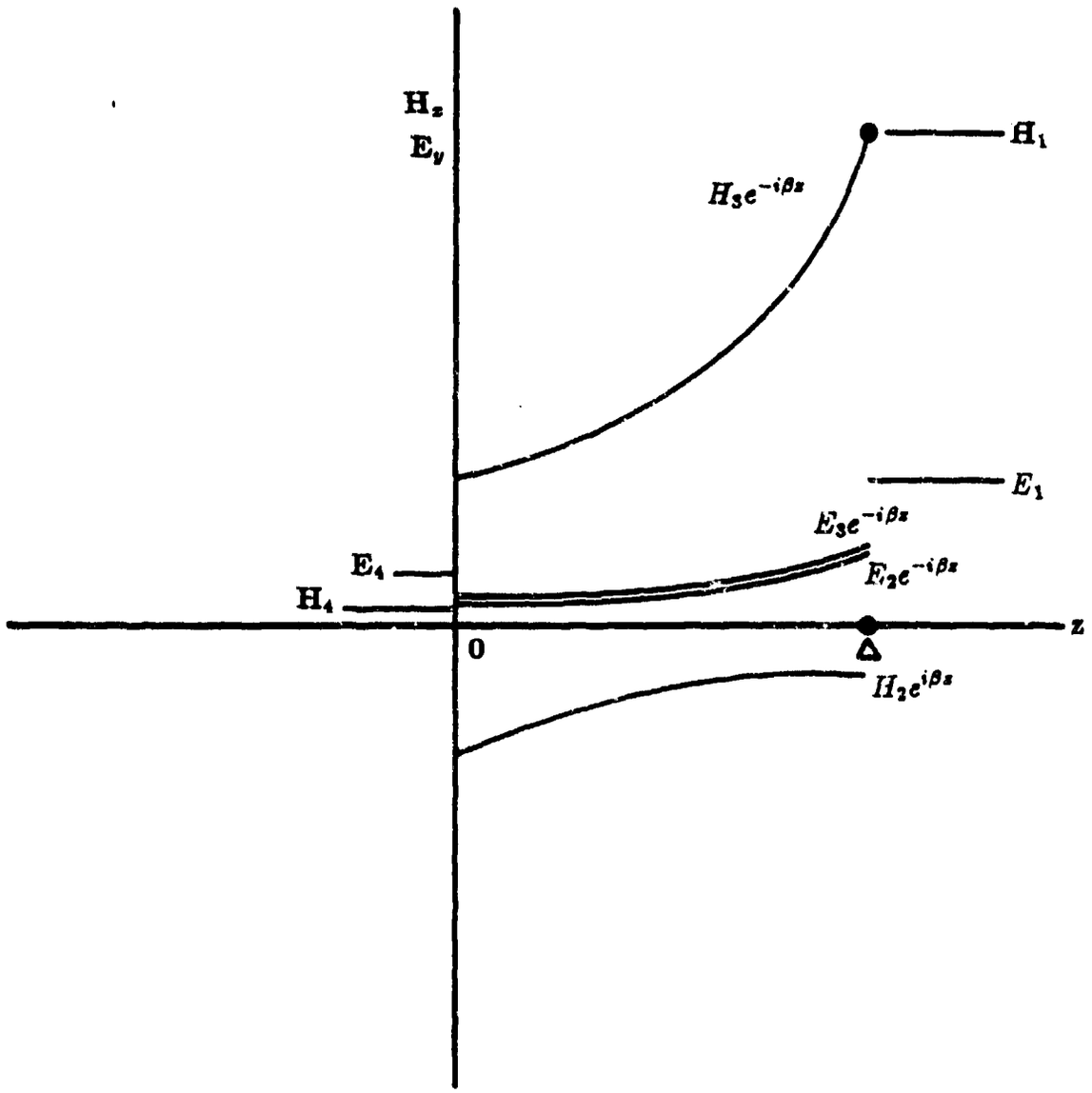

Figure 14. **Qualitative behavior of the electric and magnetic fields in figure 13 in the high frequency regime.**

field just outside the metal. To fulfill this requirement the II^2 wave is sent backward from the z = 0 surface into the conductor. Usually, the two waves in the metal have nearly equal and opposite values of H on the z = 0 surface in order to reduce the total H field. The reduction is necessary because the conductor supports waves with much larger ratios of H/E than are usually found in vacuum. The figure indicates that the backward wave magnitude is very small in the high frequency, small skin depth regime so that approximately

$$H_3 e^{-i\beta\Delta} = H_1 \quad . \tag{4-7}$$

Continuity of the electric and magnetic field at z = 0 yield

$$\begin{aligned} H_4 &= H_2 + H_3 \\ E_4 &= \frac{i\beta}{\sigma}(H_2 - H_3) \quad . \end{aligned} \tag{4-8}$$

Substituting equation 4-7 in 4-8 and solving for the internal electric field yields

$$E_4 = -\frac{2i\beta}{\sigma} e^{i\beta\Delta} H_1 + \frac{i\beta}{\sigma} H_4$$

which is the same as the more precise equation 4-3 in the high frequency limit where $|\beta\Delta| \gg 1$.

But

$$H_4 = \frac{E_4}{Z_e} \tag{4-9}$$

so that equation 4-3 yields

$$E_4 = \frac{Z_t H_1}{1 + Z_s/Z_e} \tag{4-10}$$

In many cases $Z_s/Z_e \ll 1$. In the parallel plate case, for instance, equation 3-4 in section 3 shows that

$$Z_e = i\mu_0 v \sin ka \qquad (4-11)$$

and the inequality is true provided

$$\sin ka \gg \frac{\beta}{i\mu_0 v\sigma}\frac{\cos\beta\Delta}{\sin\beta\Delta} \qquad (4-12)$$

where $k = \omega/v$.

But sin ka = 0 is the resonance condition for the modes in a parallel plate enclosure (with infinitely conducting walls). So within a very narrow frequency band about each internal mode equation 4-12 is not fulfilled. Equation 4-12 indicates the width of the band ($\Delta\omega$) is

$$\frac{\Delta\omega}{\omega_0} = \frac{\delta}{a}$$

where ω_0 is the resonance frequency given by $\sin(\frac{\omega_0 a}{v}) = 0$ and δ is the skin depth in the walls. At all other frequencies the self impedance term in equation 4-3 can be neglected and the internal electric field is very well approximated by

$$E_4 = Z_t H_1 \quad . \qquad (4-13)$$

Within the equation 4-12 frequency band, however, the impedance of the enclosure and the impedance of the conductor are very well matched so that the magnetic field H_4 within the enclosure is comparatively large. This very narrow resonance was pointed out in the section 3 discussion of the parallel plate enclosure. The method derived in the remainder of this section employs the equation 4-13 simplification and is, therefore, not valid in the narrow frequency band about each mode of the enclosure. In section 5 a method is derived to treat the narrow band of frequencies.

4.2 Calculation of E^s

Figure 15 illustrates the box with the wire running in the y direction. The E_y component of the electric field obeys the wave equation

$$\nabla^2 E_y + k^2 E_y = 0 \qquad (4-14)$$

Section A points out that in the absence of the wire the solution to this equation can be written in terms of surface integrals over the walls. It is

$$\begin{aligned} E_y(x,y,z) &= \frac{1}{4\pi}\int G\frac{\partial E_y}{\partial y'}\cdot dS'|_{x=0,a \quad z=0,c \quad \text{walls}} \\ &- \frac{1}{4\pi}\int E_y\frac{\partial G}{\partial y'}\cdot dS'|_{y=0,b\text{walls}} \end{aligned} \qquad (4\text{-}15)$$

where G

$$G = 4\pi\sum_{\substack{\ell,n=1\\ m=0}}^{\infty}\frac{8}{abc}\frac{\sin(\frac{\ell\pi x}{a})\cos(\frac{m\pi y}{b})\sin(\frac{n\pi z}{c})\sin(\frac{\ell\pi x'}{a})\cos(\frac{m\pi y'}{b})\sin(\frac{n\pi z'}{c})}{\pi^2\left[(\frac{\ell}{a})^2+(\frac{m}{b})^2-(\frac{n}{c})^2\right]-k^2}(\frac{1}{2})^{\delta_{m0}} \qquad (4-16)$$

is the Green's function which satisfies Dirichet boundary conditions on the x = constant and z = constant walls and Neumann boundary conditions on the y = constant walls.

The integrals contain E_y on the x = constant and z = constant walls. But equation 13 of the last section shows that these quantities are easily calculated. On the x = constant walls they are

$$\begin{aligned} E_y(x=0,y,z) &= +Z_t H_z \\ E_y(x=a,y,z) &= -Z_t H_z \end{aligned} \qquad (4\text{-}17)$$

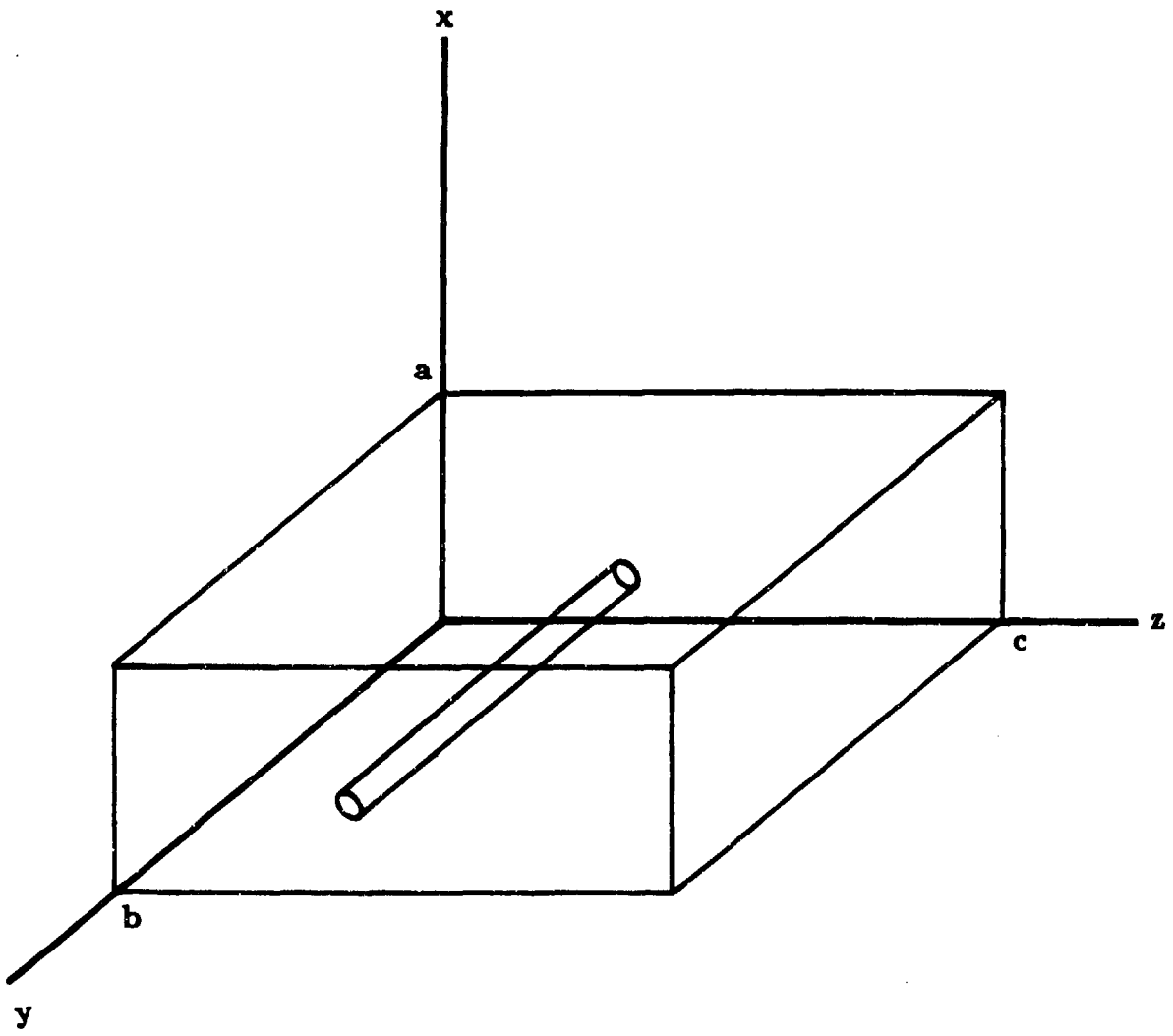

Figure 15. Box enclosure.

and on the z = constant walls they are

$$E_y(x, y, z = 0) = -Z_t H_x$$

$$E_y(x, y, z = c) = +Z_t H_x \qquad (4\text{-}18)$$

where the magnetic intensities H are on the external surfaces of the box. It is intended that the external magnetic fields will be calculated with the code HFC which is explained in section 6. HFC assumes the box has infinite conductivity and calculates H on the external surface. This is an excellent approximation. Other approximations for H on the external surfaces which avoid the use of a code are mentioned below.

On the y = constant surfaces the integral requires the normal derivative of $\partial E_y/\partial y$ at the surface. A small distance from the y = constant walls (inside the box) the divergence of the electric field is zero so that

$$\frac{\partial E_y}{\partial y} = -\frac{\partial E_x}{\partial x} - \frac{\partial E_z}{\partial z} \qquad (4-19)$$

On the y=b surface, for instance, the right hand member is derived from equation 4-13 to be

$$\frac{\partial E_x}{\partial x} = Z_t \frac{\partial H_z}{\partial x}$$

$$\frac{\partial E_z}{\partial z} = -Z_t \frac{\partial H_x}{\partial z} \qquad (4\text{-}20)$$

where H_x and H_z are the magnetic intensity on the external surface of the y=b wall. They could be supplied by the code HFC. Consequently, equation 4-15 yields the internal field E_y in terms of a quadrature over the external magnetic field. Of course, it has been assumed that the one dimensional transfer impedance in the previous section applies. This is well justified since the walls are much thinner than either the wavelength or the lengths of the box's sides. Within a very narrow frequency band around each of the box's modes this method fails. Section 5 explains how to calculate the fields within these bands.

In the most general case the external field is incident on the box at arbitrary angle and may have any spatial dependence satisfying the wave equation. HFC can treat this case and will furnish the magnetic intensity H on the external surface of the box. Equations 4-17, 4-18 and 4-19 then furnish E_y and $\partial E_y/\partial y$ from H. Finally, equation 4-15 yields E_y inside the box which is needed in the next section to calculate the wire current.

The integral in equation 4-15 is reasonably straight- forward. In some cases H approaches infinity at the edge of the box. But these are integrable singularities. In order to illustrate the method a simple example is worked out in the next subsection.

4.3 Simple Example

In order to illustrate the general method in the previous subsection consider the case of a plane wave normally incident on the z = c wall of the box in figure 15. If the wavelength is much less than the box dimensions then the geometric optics theory of light indicates that total magnetic field on the z = c face is twice that of the incident field and is constant over the surface. The surface magnetic field is smaller on the other faces. In this example it is assumed that the surface magnetic field is zero everywhere except the exposed face and is well behaved at the edges of the box.

Equation 4-18 shows that the internal electric field on the z = c wall is

$$E_y = 2Z_t H_x^i \qquad (4-21)$$

where H_x^i is the field of the incident wave generated by a source of electromagnetic interference, perhaps. The electric fields tangent to the other walls will be much less than this. Equation 4-3 shows that these electric fields can be computed from H_1 and H_4 the external and internal magnetic fields on each wall. But, by assumption H_1 is zero except on the z=c face. Consequently, the internal electric field on the other walls is given by

$$E_4 = -Z_s H_4 \qquad (4-22)$$

The internal magnetic field H_4 is roughly the same on all walls of the box. Hence, the magnitude of the internal field E_4 is about the same on all the walls. But in section 4.1 this term was shown to make a negligible correction to the internal electric field on the z =

c wall. Hence, the internal field is much larger on the exposed wall (z=c) than the others. From equation 4-19 it can be inferred that $\partial E_y/\partial y$ is small also.

Consequently, only the integral over the z = c face survives in equation 4-15 and

$$E_y(x,z) = -\frac{8Z_t H_x^i}{\pi^3 c^2} \sum_{\ell,n=1}^{\infty} \left\{ \frac{n \cos n\pi(1-\cos \ell\pi)}{\ell[(\frac{\ell}{a})^2 + (\frac{n}{c})^2 - k^2]} \right\} \sin \frac{\ell n x}{a} \sin\left(\frac{n\pi z}{c}\right) \quad . \qquad (4-23)$$

E_y is independent of y for this case.

4.4 Wire Current E^w

At each point on the wire the relationship

$$IR_0(1-i)\frac{w_0}{2\delta_0} = E^e + E^w \qquad (4-24)$$

must be satisfied. It is convenient to transform each side of this equation with a cosine transform

$$f_m = \frac{2}{2^{\delta m_0} b} \int_0^b f(y) \cos \frac{m\pi y}{b} dy$$

$$f_{(y)} = \sum_{m=0}^{\infty} f_m \cos \frac{m\pi y}{b} \qquad (4\text{-}25)$$

yielding

$$I_m R_0(1-i)\frac{w_0}{2\delta} = E_m^e + E_m^w \qquad (4-26)$$

where the subscript m indicates the m^{th} fourier coefficient.

Simple Case

First the wire current will be derived for the simple case treated in the previous section. Because the plane wave is normally incident on the box, E_y (equation 4-23) is independent of the y -coordinate and only the $m = 0$ coefficient is non-zero. It is trivially given by equation 4-23 to be

$$E^s_{m=0} = -\frac{8Z_t H^i_x}{c^2} \sum_{\ell,n=1}^{\infty} \left\{ \frac{n(\cos n\pi)(1-\cos \ell\pi)}{\ell\left[\left(\frac{\ell_\pi}{a}\right)^2 + \left(\frac{n_\pi}{c}\right)^2 - k^2\right]} \right\} \sin\left(\frac{\ell\pi x}{a}\right) \sin\left(\frac{n\pi z}{c}\right) \quad . \qquad (4-27)$$

In section A.2 the electric field E^w produced by the wire was calculated. From equation 2-25 it is clear that the $m = 0$ component is

$$E^w_{m=0} = \frac{-4\omega I_{m=0}}{iac\epsilon_0 v^2} \sum_{\ell,n=1}^{\infty} \frac{\sin^2 \frac{\ell\pi\xi}{a} \sin^2 \frac{n\pi\eta}{c}}{k_n^2 - k^2} \qquad (4-28)$$

Substituting equations 4-27 and 4-28 in 4-26 yields the wire current

$$I = \frac{\frac{-8Z_t H^i_x}{c^2} \sum_{\ell,n=1}^{\infty} \left\{ \frac{n(\cos n\pi)(1-\cos \ell\pi)}{\ell[(\frac{\ell_\pi}{a}) + (\frac{n_\pi}{c})^2 - k^2]} \right\} \sin \frac{\ell\pi\xi}{a} \sin \frac{n\pi\eta}{c}}{R_0(1-i)\frac{w_0}{2\delta_0} - \frac{4i\omega}{ac\epsilon_0 v^2} \sum_{\ell,n=1}^{\infty} \frac{\sin^2 \frac{\ell\pi\xi}{a} \sin^2 \frac{n\pi\eta}{c}}{k_n^2 - k^2}} \qquad (4-29)$$

General Case

For an arbitrary incident wave the code HFC (section 6) furnishes the magnetic intensity H on the external surface. Equations 4-17, 4-18 and 4-19 then yield the internal electric field on all surfaces which are used in 4-15 to yield the internal electric field at the wire E^w. The Green's function in equation 4-15 contains the factor $\cos \frac{m\pi y}{b}$. Hence, this formalism will always furnish E^e as a cosine transform of the form

$$E^e = \sum_{m=0}^{\infty} E_m^e \cos \frac{m\pi y}{b}$$

Of course, E_m^w will contain the integrals in equation 4-15 but these are straightforward to perform numerically in the general case.

From 2-25 the m^{th} fourier coefficient of E^w is

$$E_m^w = \frac{-4I_m}{i\omega ac\epsilon_0} \sum_{\ell,n=1}^{\infty} \frac{\left[\frac{\omega^2}{v^2} - \left(\frac{m\pi}{b}\right)^2\right]}{k_n^2 - k^2} \sin^2 \frac{\ell\pi\xi}{a} \sin^2 \frac{n\pi\eta}{c}$$

Equation 4-26 then yields the m^{th} Fourier coefficient of the wire current

$$I_m = \frac{E_m^e}{R_0(1-i)\frac{w_0}{2\delta_0} - \frac{4i}{\omega ac\epsilon_0} \sum' \frac{\left[\frac{\omega^2}{v^2} - \left(\frac{m\pi}{b}\right)^2\right]}{k_n^2 - k^2} \sin^2 \frac{\ell\pi\xi}{a} \sin^2 \frac{n\pi\eta}{c}}$$

Finally, the current I in the wire at any position is given by summing the Fourier components

$$I = \sum_{m=0}^{\infty} I_m \cos \frac{m\pi y}{b}$$

The calculation is straightforward, but tedious. It is expected to be valid except in the narrow frequency band about each internal mode of the box. The behavior of the fields at the edges of the box should be considered more thoroughly.

SECTION 5

HIGH FREQUENCY REGIME - COMPLETE TREATMENT

It has been pointed out that the section 4 method does not apply in a very narrow frequency band centered about each mode of the enclosure. Within the band the internal magnetic field H^4 (equation 4-3) is driven to comparatively large values and the internal electric field is not accurately approximated by $Z_t H_1$. The internal electric and magnetic fields must be calculated self consistently. A method of calculating the wire current in this situation is outlined in this section.

Consider the H_z component of the internal magnetic intensity which in the absence of the wire satisfies the homogeneous Helmholtz equation

$$\nabla^2 H_z + \frac{\omega^2}{v^2} H_z = 0 \qquad (5-1)$$

In terms of the magnetic intensity at the inside surface of the walls section A points out

$$H_z = \frac{-1}{4\pi} \int dS' \cdot H_z \nabla' G \qquad (5-2)$$

where the surface integrals are taken over the x = constant and y = constant walls. Because H_z is normal to the z = constant walls it is very small on these surfaces and is neglected. The Green's function satisfies Dirichlet boundary conditions

$$G = 4\pi \left(\frac{abc}{8}\right) \sum_{\ell,m,n=1}^{\infty} \frac{\sin \frac{\ell\pi x}{a} \sin \frac{m\pi y}{b} \sin \frac{n\pi z}{c} \sin \frac{\ell\pi x'}{a} \sin \frac{m\pi y'}{b} \sin \frac{n\pi z'}{c}}{k_n^2 - k^2} \qquad (5-3)$$

The electric field tangent to these four interior walls can be fourier decomposed into

$$E_y(0,y,z) = \sum_{m,n=1}^{s} e_{y0}^{mn} \sin\frac{m\pi y}{b} \sin\frac{n\pi z}{c}$$

$$E_y(a,y,z) = \sum_{m,n=1}^{s} e_{ya}^{mn} \sin\frac{m\pi y}{b} \sin\frac{n\pi z}{c}$$

$$E_x(x,0,z) = \sum_{\ell,n=1}^{s} e_{x0}^{\ell n} \sin\frac{\ell\pi x}{a} \sin\frac{n\pi y}{c}$$

$$E_x(x,b,z) = \sum_{\ell,n=1}^{s} e_{xb}^{\ell n} \sin\frac{\ell\pi x}{a} \sin\frac{n\pi z}{c} \qquad (5\text{-}4)$$

Equation 4-3 indicates that the the x = 0 wall

$$H_s = \frac{\sigma}{i\beta} E_x + 2H_1 e^{i\beta\Delta} \qquad (5-5)$$

where H_1 is the external field on the surface of the box which is computed by the code HFC (section 6). On the x = a, y = 0,b walls analogous equations furnish the interior surface electric fields.

In addition, on the y = b wall Faraday's law shows

$$E_x = \frac{-4\pi}{i\omega\epsilon_0} \frac{\partial H_s}{\partial y} \quad . \qquad (5-6)$$

Substituting, equations 5-4, 5-5, 5-6 into 5-3 yields

$$-4\pi e_{xb}^{\ell n} = \sum_{m=1}^{s} \frac{4\pi}{i\omega\epsilon_0} \left(\frac{abc}{8}\right) \frac{\cos m\pi}{k_n^2 - k^2}$$

$$\left\{ 2e^{i\beta\Delta} \frac{\ell\pi}{a} \cos\ell\pi \frac{4}{bc} H_1^{m,n}(x=a) \right.$$

$$+ \quad \frac{\ell\pi}{a}\cos\ell\pi\frac{\sigma}{i\beta}\frac{bc}{4}e_{ya}^{mn}$$

$$- \quad 2e^{i\beta\Delta}\frac{\ell\pi}{a}\frac{4}{bc}H_1^{mn}(x=0) - \frac{\ell\pi}{a}\frac{\sigma}{i\beta}\frac{bc}{4}e_{y0}^{mn}$$

$$+ \quad 2e^{i\beta\Delta}\frac{m\pi}{b}\cos m\pi\frac{4}{ac}H_1^{\ell n}(y=b) + \frac{m\pi}{b}\cos m\pi\frac{\sigma}{i\beta}\frac{ac}{4}e_{xb}^{\ell n}$$

$$- \quad 2e^{i\beta\Delta}\frac{m\pi}{b}\frac{4}{ac}H_1^{\ell n}(y=0) - \frac{m\pi}{b}\frac{\sigma}{i\beta}\frac{ac}{4}e_{x0}^{\ell n}\Bigg\} \quad . \tag{5-7}$$

Here the Fourier components on the x=a wall of the field H_1 is denoted by $H_1^{mn}(x = a)$. Other components of H_1 are denoted by a similar notation.

This equation relates $e_{ya}^{mn}, e_{y0}^{mn}, e_{xb}^{\ell n}, e_{x0}^{\ell n}$ and the H^1 components given by the code HFC on the $x = 0,a$ and $y = 0,b$ walls. Equations 5-4 have $4S^2$ unknown Fourier coefficients. Equation 5-7 is S^2 equations relating these unknowns. $3S^2$ more equations are found by applying the same method to calculate H_s on the $y = 0$ and $x = 0,a$ planes. Solving these simultaneous algebraic equations numerically furnishes all the coefficients in equations 5-4. Some care must be exercised when evaluating the series expressions near the edges since they may converge slowly.

Applying the same technique to the H_x and H_y counterparts of equation 5-1 allows a self consistent calculation for the internal electric field tangential to all the internal surfaces of the box. From these E^s can be computed. Section 2 yields E^w which can then be employed with

$$IR_0(1-i)\frac{w_0}{2\delta_0} = E^s + E^w$$

to furnish the wire current as in sections 2, 3 and 4.

SECTION 6

HIGH FREQUENCY CODE

A rectangular box illuminated by electromagnetic radiation can be described in terms of the magnetic fields or alternatively in terms of the surface current density K. A careful analysis, yields the equation:[5]

$$\vec{K}(\vec{r}) - 2\int \hat{n} \times \vec{K} \times G(\vec{r},\vec{r}')dS' = 2\ \hat{n} \times \vec{H}^{ext}(\vec{r}) \qquad (6-1)$$

where $\vec{K}$ is the surface current, $\vec{H}^{ext}$ is the external magnetic field and G is the outgoing Green function

$$G(\vec{r},\vec{r}') = \frac{1}{4\pi|\vec{r}-\vec{r}'|\exp(ik|\vec{r}-\vec{r}'|)} \qquad (6-2)$$

corresponding to frequency $\omega = kV$. The integral over S' is over all the faces of the rectangular enclosure. Note that only the tangential component of the incident field contributes to the formation of current on the surface. The enclosure walls are infinitely conductive.

In order to solve the integral equation (6-1) for $\vec{K}$ we have written a computer code called High Frequency Code (HFC). This code solves the integral equation above numerically using finite difference approximation to the double integral. In principle, the code permits as fine a resolution of the surface as necessary because of the utilization of virtual memory in the computer. In practice, the resolution is limited by both the accuracy that can be obtained inverting a large matrix and by the amount of computer time available. Thus accuracy limits the resolution to 36 elements per face in single precision arithmetic and to about 200 elements per face in double precision arithmetic. The time required for computation increases as the third power of the total number of surface elements used. For a 4 MIPs machine, 100 elements per face requires about 1 hour of CPU time which costs about $20 on an ELXSI minicomputer.

In general HFC can treat any angle of incidence and any frequency. Round off error, however, may prevent HFC from treating frequency greater than about ten gigahertz for boxes about one meter on each side.

For the present problem we have considered only a rectangular box. Other box geometries could be also computed but the algebra becomes somewhat more involved. For the six faces of the box, there are 12 independent components of the current together with the boundary conditions at the edges of the box which arise from continuity. Each component is complex and the physical current is the real part of the product K exp(iωt).

The resultant matrix equation can be cast in the form:

$$AK = D$$

where A is the LHS matrix (kernel) and D is the driving term. In order to save memory, we had hoped that the kernel has some evident symmetries that permit more efficient computation. However, as it turns out, the matrix A is band structured, but not evidently symmetric (or antisymmetric). Thus the computation of the surface currents requires large memory available unless we invoke the physical symmetries, which though not apparent must be present in the solution. These include rotational and transinational symmetries which are clearly embedded in the original Maxwells equations. Our calculations indicate that these are indeed satisfied by our numerical solutions.

To test the validity of the code we have computed the surface currents on a long rectangular box. For this situation and an incidence perpendicular to the long axis of the box, the solution has been computed previously e.g. by Mei and van Bladel.[8] Their results together with our computations are shown in figure 16. In view of our finite resolution in the finite difference scheme the agreement with their results is excellent. The results are somewhat less accurate for the E wave, i.e. one where the magnetic field is perpendicular to the long axis of the cylinder. This is because the surface current, and the induced magnetic field is now discontinuous and divergent the edges perpendicular to the magnetic field. This can be seen in figure 17 where we show results from reference 8 for this case. We have attempted to compute this problem with our code with some success, but to obtain accurate results requires more time than we have presently available.

6.1 CODE DESCRIPTION

The basic tenet that has been used in designing the HFC code was to maintain minimum complexity, in particular since code development was not our primary goal for this effort. For this reason the code contains minimum "bells and whistles" coding. The

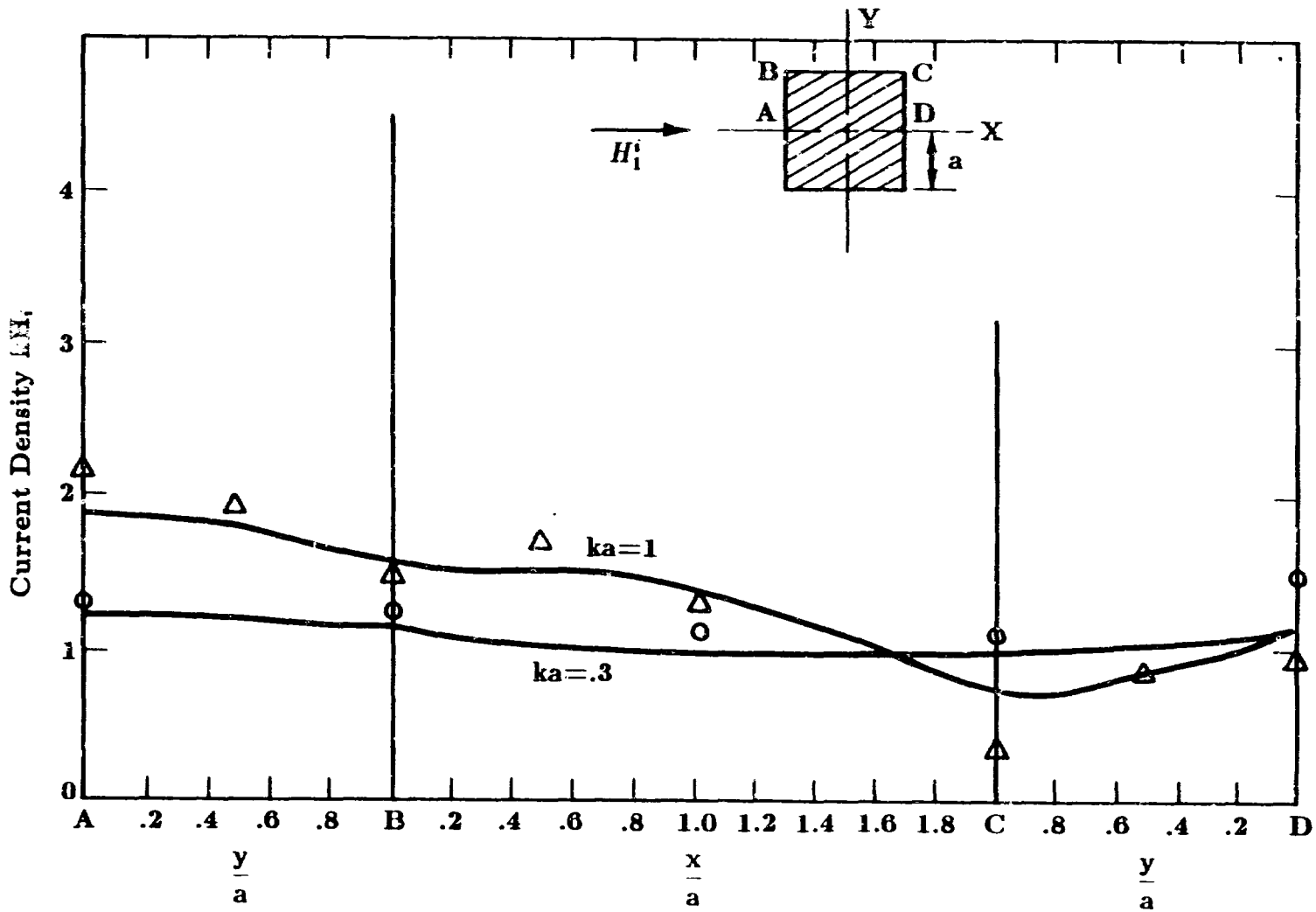

Figure 16. Surface current on a long square box in an H wave. The triangles correspond to ka=1, circles to ka=.3. The solid lines are square cylider calculations of Reference 8.

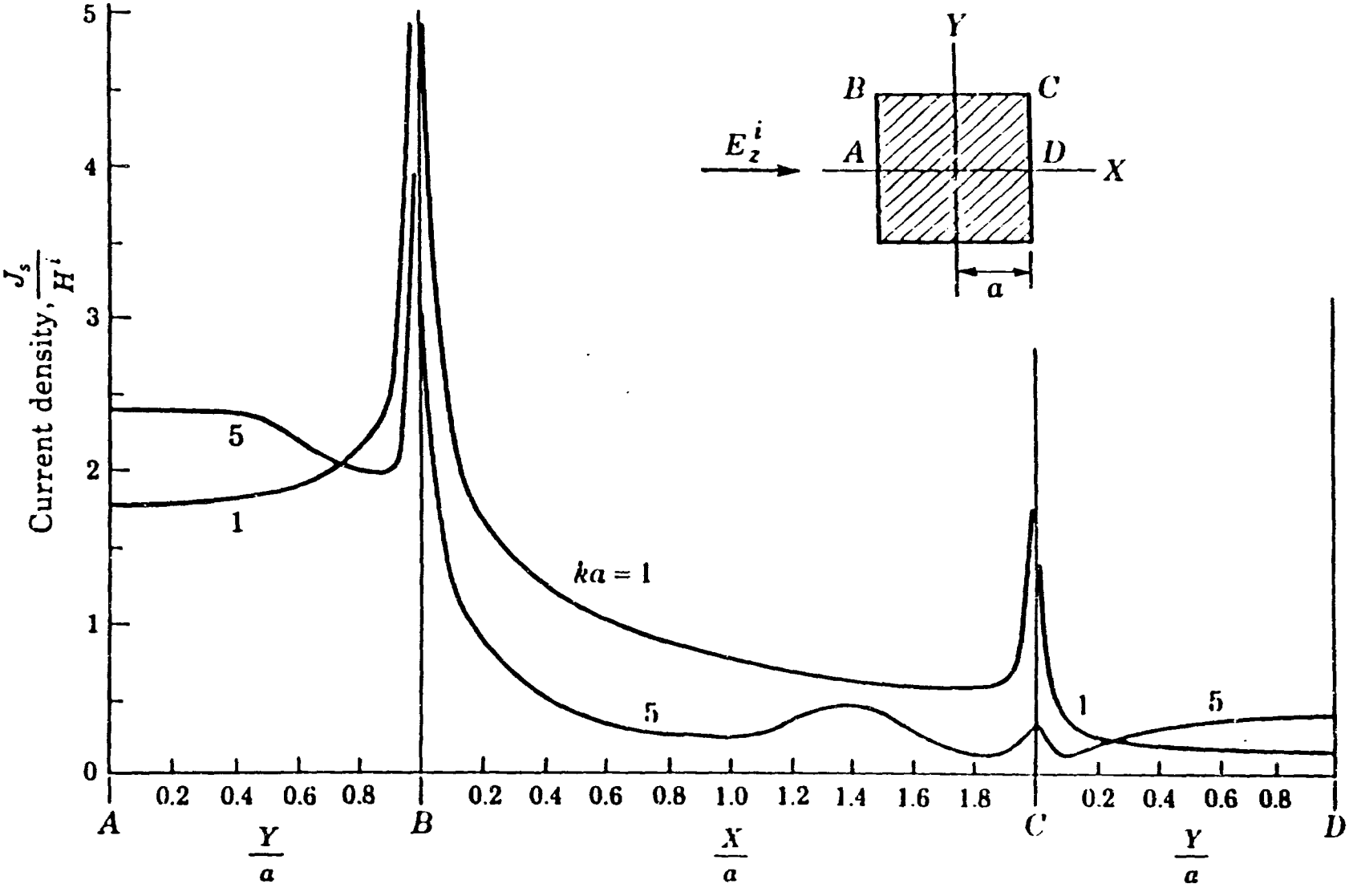

Figure 17. Surface current density for a square cylinder in an E wave. (Taken from Refererence 8.) Note the singular behavior near the edges.

input consists of the dimensions of the enclosure, frequency of incident radiation and the size of the driver field. In addition, the input requires the number of vertices in each independent direction x, y, z.

The code consists of the main control program, which defines the loop structure necessary to compute the surface integrals, the calls to the algebraic equation solver routines and the output instructions. The code uses the LINPACK GESL routine to solve the algebraic equations for $\vec{K}$ in complex arithmetic. A GREEN subroutine is used to compute the green function and its derivatives needed in equation 6-1.

The running time for the code has been obtained from a number of numerical experiments. We conclude that the CPU time required,

$$\text{CPUTIM} = \text{TZERO}(\text{nx} * \text{ny} + \text{nx} * \text{nz} + \text{ny} * \text{nz})^3,$$

where TZERO = 1.6^{-4} seconds for our 4 MIP ELXSI computer.

SECTION 7

REFERENCES

1. "Electromagnetic Field Coupling to a Wire Inside a Metallic Enclosure," Bart Goldstein, Rudolf Goldflam, Mission Research Corporation (SBIR Proposal) January 1987.

2. G. Bedrosian and K.S. H. Lee, "EMP Penetration through Metal Skin Panels," Air Force Weapon Laboratory Interactive Note 314, AFWL, Albuquerque, N.M. (August 1976.)

3. J. D. Jackson, Classical Electrodynamics, John Wiley and Sons, Inc., (1962).

4. R. W. Latham and K.S.H. Lee, "Theory of Inductive Shielding", Air Force Weapons Laboratory, EMP Note 12, AFWL, Albuquerque, N.M. (March 1968).

5. K.S.H. Lee, EMP Interaction: Principles, Techniques and Response Data, AFWL-TR-80-402. Air Force Weapons Laboratory, Albuquerque, N.M. (1980).

6. J.A. Stratton, Electromagnetic Theory, McGraw Hill Book Company, New York, 1941.

7. J. Van Bladel, "Electromagnetic Fields," Springer (1985).

8. K. Mei and J. Van Bladel, IEEE Trans. Antennas and Propagation, 11, 185 (1963).

APPENDIX A

INTRODUCTION

A.1 Summary of Results

Electromagnetic radiation can diffuse through a thin walled metallic box and couple to internal circuitry. At high frequencies for which the skin depth is much smaller than the wall thickness a metallic enclosure is a good shield. At low frequencies, however, the incident magnetic field penetrates the walls easily so that the magnetic field within the box approaches the magnitude of the external field radiating the enclosure. This report discusses the diffusion of a low frequency electromagnetic signal through a thin walled box that contains a wire which is connected between opposite walls of the parallelpiped (figure A-1). A quantitative analytic theory is derived to predict the current on the wire. Easily applied formulas are found which furnish the wire current as a function of time due to any external driving pulse. Frequency domain solutions for the wire current are also shown. In order to establish the theory's credibility its predictions are compared to the wire current calculated by the code BOX4.

The theory developed below indicates that the current I(amperes) in the wire is given by

$$I(\omega) = \frac{i\mu_0\omega H^e}{R - i\omega\mathcal{L}}\left[xL - \frac{wL(L+2x)}{2(w+L)}\right] \qquad (A-1)$$

where ω is the frequency of the external radiation incident on the enclosure, R is the wire resistance, $\mathcal{L}$ is the wire inductance and the box dimensions and wire location are denoted by w,L,x as in figure A-2. The permiability of space is μ_0 and $i = \sqrt{-1}$. H^e, the magnetic field intensity within the box is approximated by

$$H^e = \left[\frac{1}{1 - \frac{i\omega\mu_0\sigma\Delta s}{3}}\right] H^D \qquad (A-2)$$

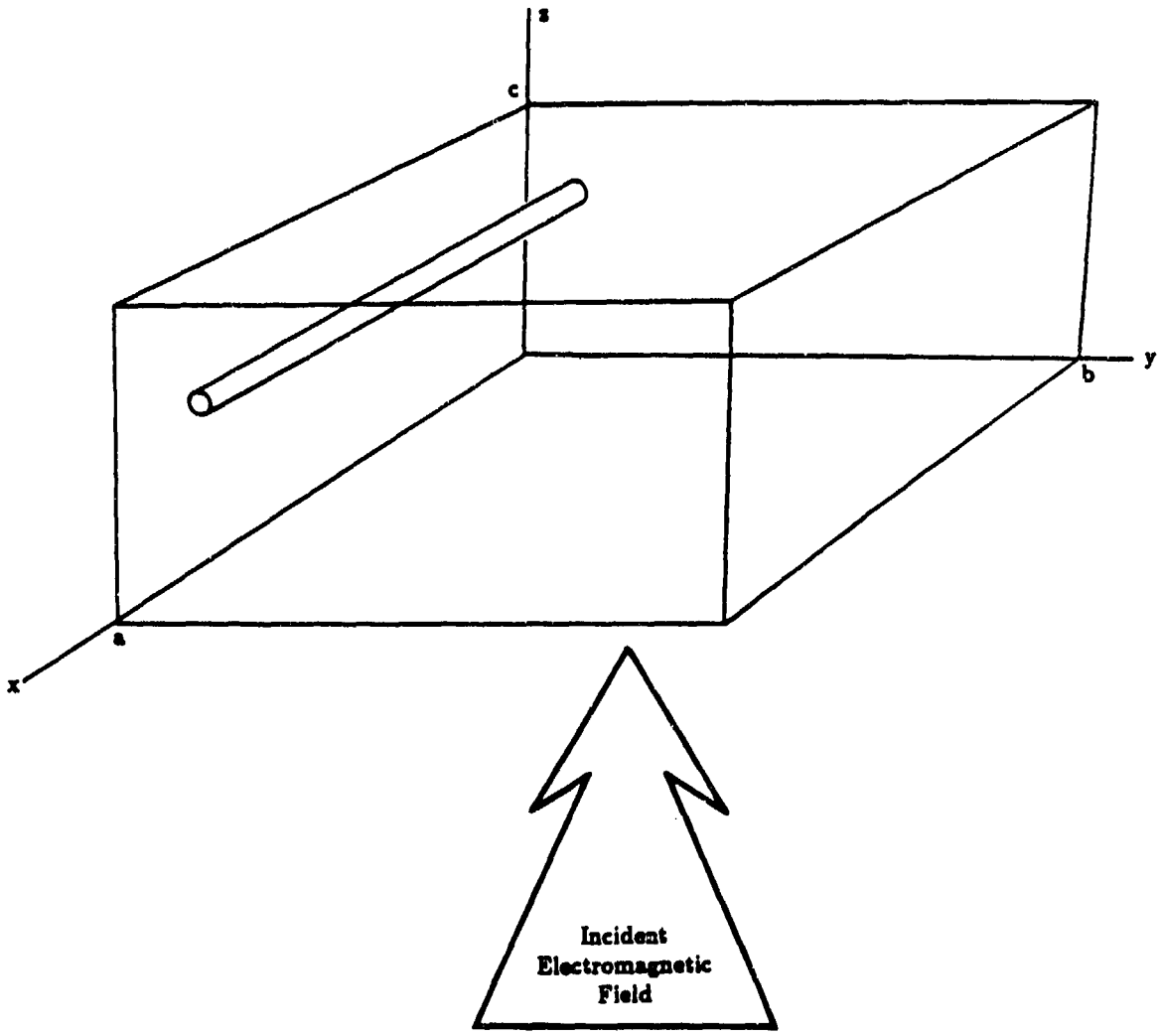

Figure A-1. The incident electromagnetic wave diffuses through the box and induces a current on the internal wire.

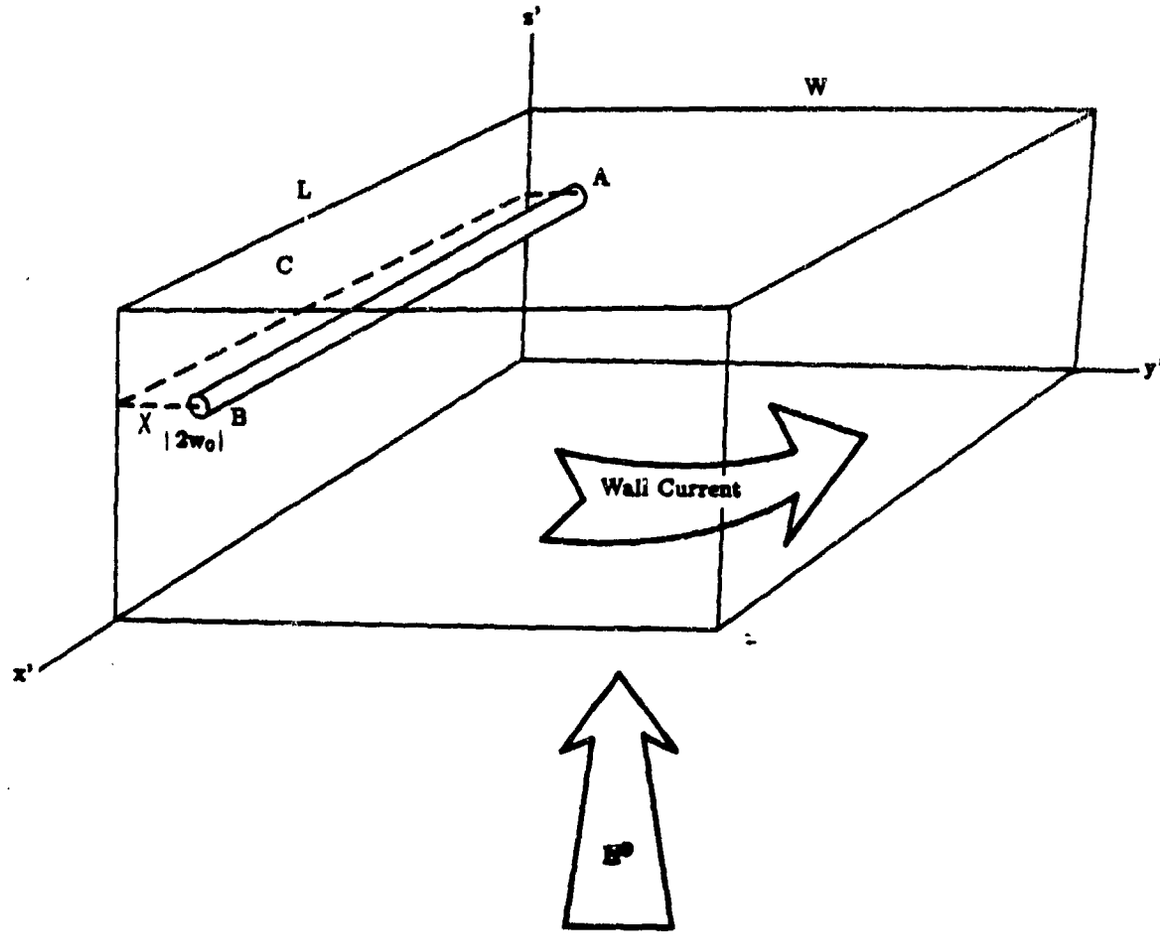

Figure A-2. Problem geometry.

where σ is the conductivity of the walls, and Δ is the wall thickness. The external magnetic field radiating the box is assumed to be the real part of

$$H^D e^{-i\omega t} \quad .$$

Because the wavelength of the low frequency radiation is much larger than the box H^D is independent of position in the vicinity of the enclosure. The parameter a is

$$a = \left(\frac{3V}{4\pi}\right)^{1/3}$$

in terms of the volume V of the enclosure. MKS units are used throughout this report.

Figure A-3 compares the wire current predicted by these expressions with the current computed by the computer code BOX4 discussed below. The agreement is within a factor of four over five orders of magnitude of frequency. At one hertz angular frequency the code and analytic method differ by six percent and at 100000 hertz the analytic predictions are a factor of four too small. In this example the box is two meters on each side and its walls are one millimeter thick. The wall conductivity is $\sigma = 10^6$ (mho/meter). The wire resistance is 0.0366 ohms and it is one-half meter from the $y'=0$ and $z'=0$ walls. The wire is one centimeter in radius and the external magnetic field is perpendicular to the wire and has a magnitude of one ampere/meter.

Table A-1 indicates that equations A-1 and A-2 predict the wire current at different positions of the wire at one hertz angular frequency. Agreement is within twenty percent when the wire is varied between five centimeters from the wall and five centimeters from the center of the box which is 2 meters on each side. All other parameters are identical to the figure A-3 case.

Table A-2 indicates that at 100000 hertz the analytic method correctly evaluates the dependence of wire current on wire position. As the position is varied the analytic prediction is always about a factor of three smaller than the code. The analytic method always underpredicts the current by the same factor at high frequency regardless of wire position. As in figure A-3 the disagreement at high frequency is due to the approximations made in the derivation equations A-1 and A-2.

More extensive comparisons are necessary to evaluate the accuracy of the analytic formulas over a large range of box dimensions, wire parameters and wall conductivity

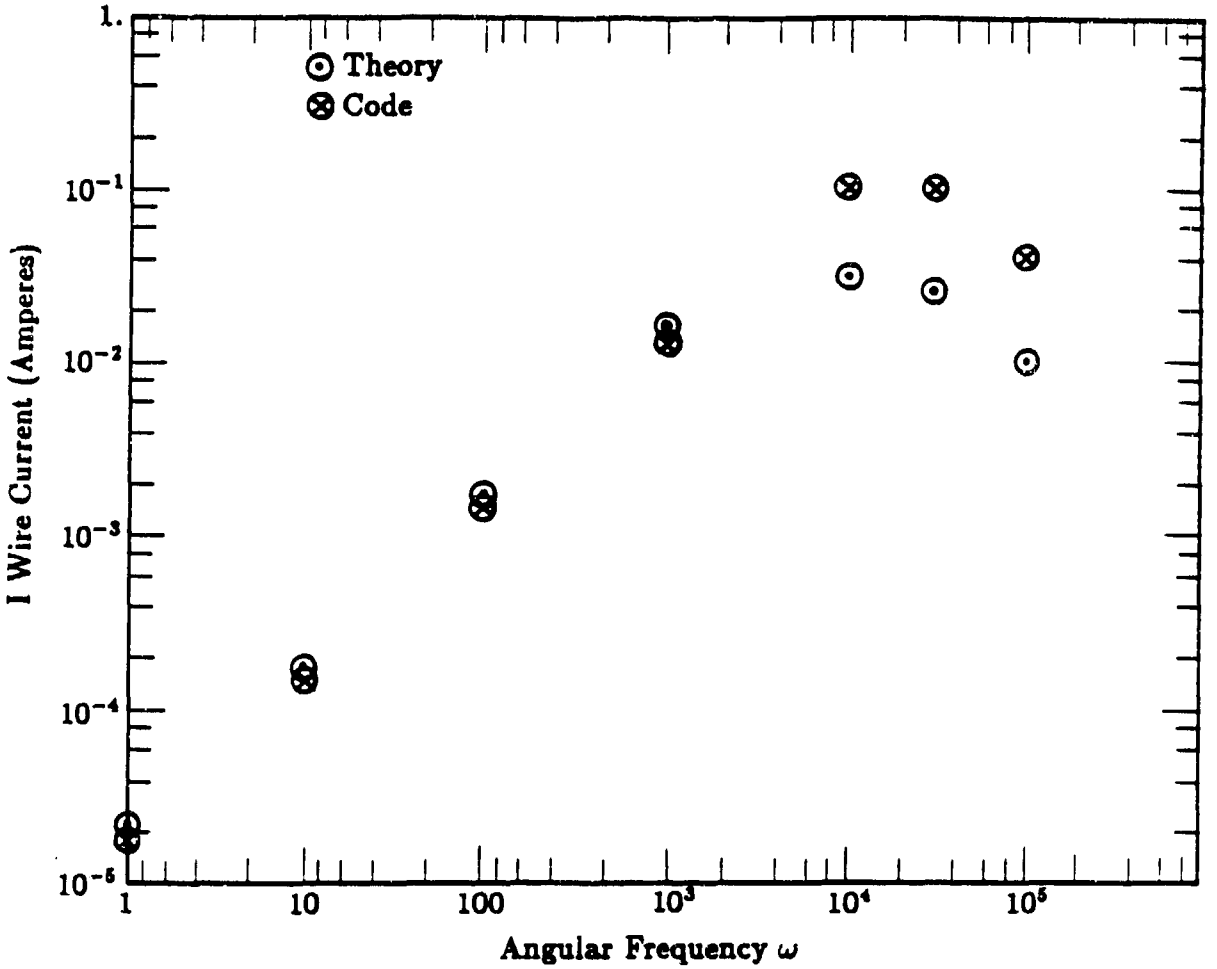

Figure A-3. Wire current.

Table A-1. Wire current as a function of wire position.

Wire Position x (cm)	Wire Current Theory (Amp)	Wire Current Code (Amp)
5	3.3×10^{-5}	3.5×10^{-5}
10	3.1×10^{-5}	3.3×10^{-5}
50	1.7×10^{-5}	1.6×10^{-5}
95	1.7×10^{-6}	1.4×10^{-6}

Table A-2. Wire current as a function of wire position.

Wire Position x (cm)	Wire Current Theory (Amp)	Wire Current Code (Amp)	Ratio Code ÷ Theory
5	0.033	0.10	3.0
10	0.027	0.081	3.0
50	0.011	0.043	3.9
95	0.0011	0.0029	2.6

and thickness. These results suggest, however, that the basic physics of the situation is contained in the equations and they are sufficiently accurate for many purposes. The results are typical in so far as the wire resistance is comparable to the inductive reactance at intermediate frequencies and the wall thickness and conductivity are realistic. These are all the comparisons made to date.

The code BOX4 should predict the wire current even in situations for which the analytic method is insufficiently accurate to be useful. Because it is comparatively inexpensive to run (cf. section A.3) it may be helpful in many problems.

In the remainder of section A.1 the analytic method equations are derived and the basic characteristics of the wire current are explained in both the frequency and time domain. Sections A.2-A.5 of the report are concerned with the description of the code BOX4. The last section discusses progress made in treating very high frequency incident radiation.

A.2 Diffusion and Coupling Fundamentals

The low frequency shielding of a metallic enclosure can be understood by considering the case of a spherical metallic shell exposed to a spatially homogeneous uniform external magnetic field of intensity H^D at frequency ω (figure A-4). At frequencies much lower than the natural modal frequencies of the sphere the displacement current can be neglected (section A.4) and the internal field satisfies

$$\nabla \times H^e = 0 \quad . \qquad (A-3)$$

Within the shell having conductivity σ and thickness Δ a current flows parallel to the spherical surface

$$J = \sigma E$$

where E is the electric field. Integrating across the thickness Δ of the thin sheet yields the surface current density K (amperes/meter)

$$K = \sigma \Delta E \qquad (A-4)$$

This current creates its own magnetic field which subtracts from that of the incident wave reducing the field inside the shield. The change in the tangential component of the magnetic intensity across the shield is, of course

$$H^D - H^e = K \qquad (A-5)$$

while the component normal to the shield is continuous through it. Finally, the electric field in the shield is associated with the rate of change of magnetic flux in the shield by Faraday's law

$$\nabla \times E = -\mu_0 \frac{\partial H}{\partial t} \qquad (A-6)$$

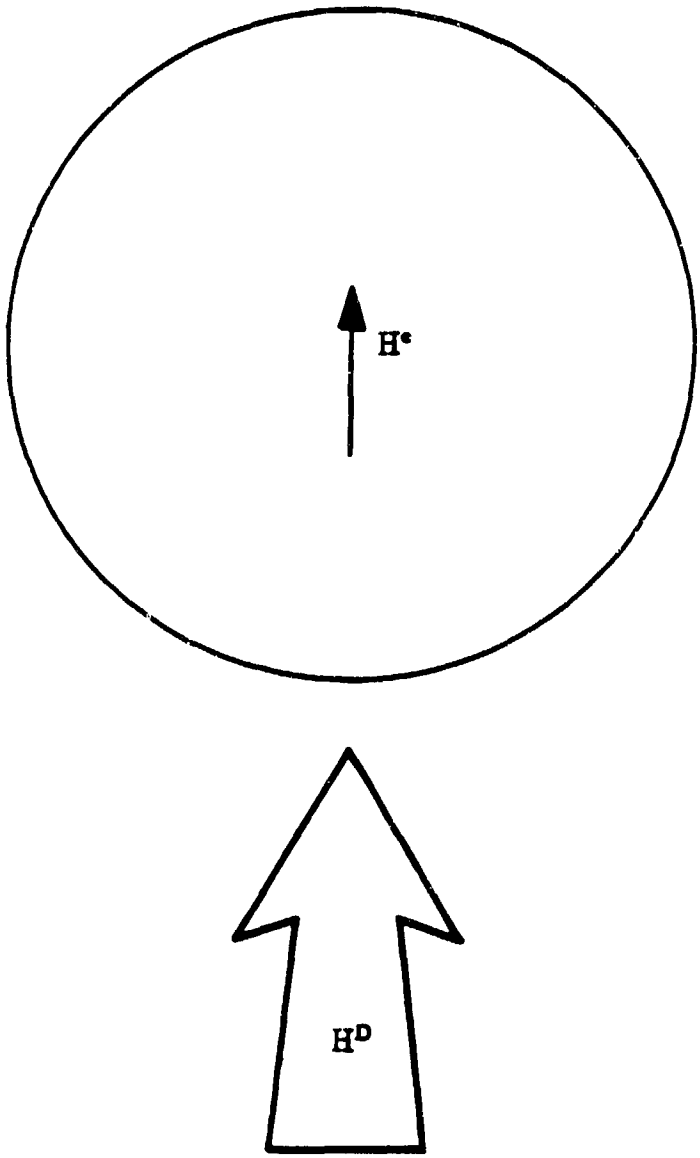

Figure A-4. Spherical shell in an incident magnetic field.

It is easily shown that the solution to equation A-3 through equation A-6 is the internal magnetic field

$$H^e = \left[\frac{1}{1 - \frac{i\omega\mu_0\sigma\Delta a}{3}}\right] H^D$$

This internal field is parallel to the external field and also spatially homogeneous (uniform).

Clearly, at frequencies lower than

$$\omega_1 = \frac{3}{\mu_0\sigma\Delta a} \qquad (A-7)$$

the internal field almost equals the external field because the slowly changing magnetic field induces a small electric field (equation A-6) which drives little current K in the shield. But at frequencies higher than ω_1 a large current K causes a small internal field. Above the cut off frequency ω_1 the internal field decreases inversely with ω and oscillates ninety degrees out of phase with the external driver. This behavior is called inductive shielding to distinguish it from the shielding which occurs at sufficiently high frequencies

$$\omega \gg \omega_2$$

$$\omega_2 = \frac{1}{\mu_0\sigma\Delta^2} \qquad (A-8)$$

that the skin depth is less than the wall thickness. In inductive shielding the electric field through the wall is nearly uniform as is the wall current it drives. All but the last section of this report is concerned with inductive shielding and frequencies well below both the modal frequencies of the enclosure or ω_2.

Several useful characteristics of the spherical case apply to all enclosures regardless of their shape. Firstly, above a cutoff frequency (approximately ω_1) the internal field always decreases inversely with the frequency. Although the field is not the same at each point it decreases by the same factor at each point as the frequency increases (above the cutoff frequency). In other words, the internal field is of the form

$$H^e(\bar{r}) = \frac{1}{\omega} f(\bar{r})$$

where $f(\bar{r})$ is the spatial dependence of the field and the frequency enters only as an overall coefficient. This is proven rigorously for any shape enclosure in section A.3. Another important characteristic is that the internal fields are approximately spatially uniform so $f(\bar{r})$ is approximately constant. In the cases of a sphere, cylinder and a parallel plate enclosures the internal field is exactly the same at all points[3]. This is obvious at very low frequencies where the walls do not shield effectively and the internal and external fields are the same. As the frequency increases the field in these simple geometries remains uniform. In the general case, of course, the fields will vary somewhat within the enclosure but as long as the shape is not radically different from a sphere, cylinder or two parallel plates one would expect the internal field to be approximately uniform. At very high frequencies, of course, the internal fields are very non-uniform since the cavity modes are excited.

In summary, the analytic theory in section A.1 assumes that the field in the box is approximately spatially homogeneous as it is for a sphere, cylinder and two parallel plates. It might be pointed out that the internal field in these three cases differ only by about a factor of two. The theory assumes that the shielding of a box must be quite similar and the internal field is approximated by the field in a sphere having the same volume as the box (equation A-2).

Equation A-1 which estimates the wire current is derived by integrating Faraday's law around the dotted line closed path in figure A-2

$$\oint \mathbf{E} \cdot d\boldsymbol{\ell} = i\omega\mu_0 \int \mathbf{H} \cdot \mathbf{n} dS$$

The line integral can be divided into a part through the wire and a part through the walls

$$\int_A^B \mathbf{E} dx = IR$$

$$\int_{BCA} \mathbf{E} \cdot d\boldsymbol{\ell} = V_d$$

where I and R are the wire current and resistance, respectively. The paths A–B and B–C–A are indicated in the figure. The total internal magnetic field H is the sum of the field

produced by the current in the wire H^w and the field which diffuses through the shield H^e. Consequently, $H = H^w + H^e$ and

$$IR + V_d = i\omega\mu_0 \int H^w \cdot ndS + i\omega\mu_0 \int H^e \cdot ndS \qquad (A-9)$$

This equation is proven rigorously in section A.2.

It was pointed out that the magnetic field within the box is roughly uniform so that

$$\int H^e \cdot ndS = H^e Lx$$

where x and L are defined in figure A-2. Consider a contour of integration in the walls which circles the box like the wall current (figure A-2). The magnetic flux through the contour is HwL so the average field in the walls must be

$$E_w = +\frac{\mu_0 wL}{2(w+L)} i\omega H^e$$

Hence,

$$V_d = E_w(L + 2x)$$

and

$$IR + i\omega H^e \frac{\mu_0 wL(L+2x)}{2(w+L)} = i\omega\mu_0 \int H^w \cdot ndS + i\omega\mu_0 H^e Lx \qquad (A-10)$$

The flux produced by the wire linking the path of integration is proportional to the inductance $\mathcal{L}$ of the wire

$$\mathcal{L}I = -\mu_0 \int H^w \cdot ndS \qquad (A-11)$$

Consequently

$$IR + i\omega \mathcal{L} I = i\mu_0 \omega H^e \left[xL - \frac{wL(L+2x)}{2(w+L)} \right] \qquad (A-12)$$

This is equation A-2. The authors[1] original derivation of this equation assumed that $\mathcal{L}$ is the inductance of a wire in free space. Recent work has shown that the free space inductance is about a factor of three too large if the wire is near the center of the box. In section A.4 the inductance is calculated accurately. Figure A-5 which graphs the inductance for the table A-2 case shows that it depends slightly on the wire location and is approximately the free space inductance. In the section A.1 comparisons the more accurate values of inductance were employed.

Clearly, several approximations have been made to deduce the final results. The most controversial are probably the assumption that the internal fields are uniform and approximated by a sphere. The authors believe these are indeed general features of low frequency diffusion. The code comparisons support this intuitive judgement convincingly but much more extensive comparisons are needed.

A.3 General Characteristics of the Wire Current

Equation A-9 has a simple interpretation. The right hand member of the equation is the EMF linking the loop in figure A-3. It is the driver of the wire current. The wire inductance L is a source of back EMF which reduces the wire current.The equation indicates that the total EMF drops through the wire resistance R and the wall resistance. The path of the loop in the walls is, of course, arbitrary but once a path has been chosen both the driver and V_d must be computed with that path.

The wire current dependence on frequency is typified by figure A-3. At low frequencies the current is small because the electric field induced by the slowly changing magnetic field produces a small EMF (right hand member of equation A-9). As the frequency increases the EMF and wire current increase. At the frequency ω, however, the wall current begins to effectively reduce the magnetic field in the enclosure so the EMF increases less rapidly with increase in frequency. For frequencies larger than a few times the critical frequency

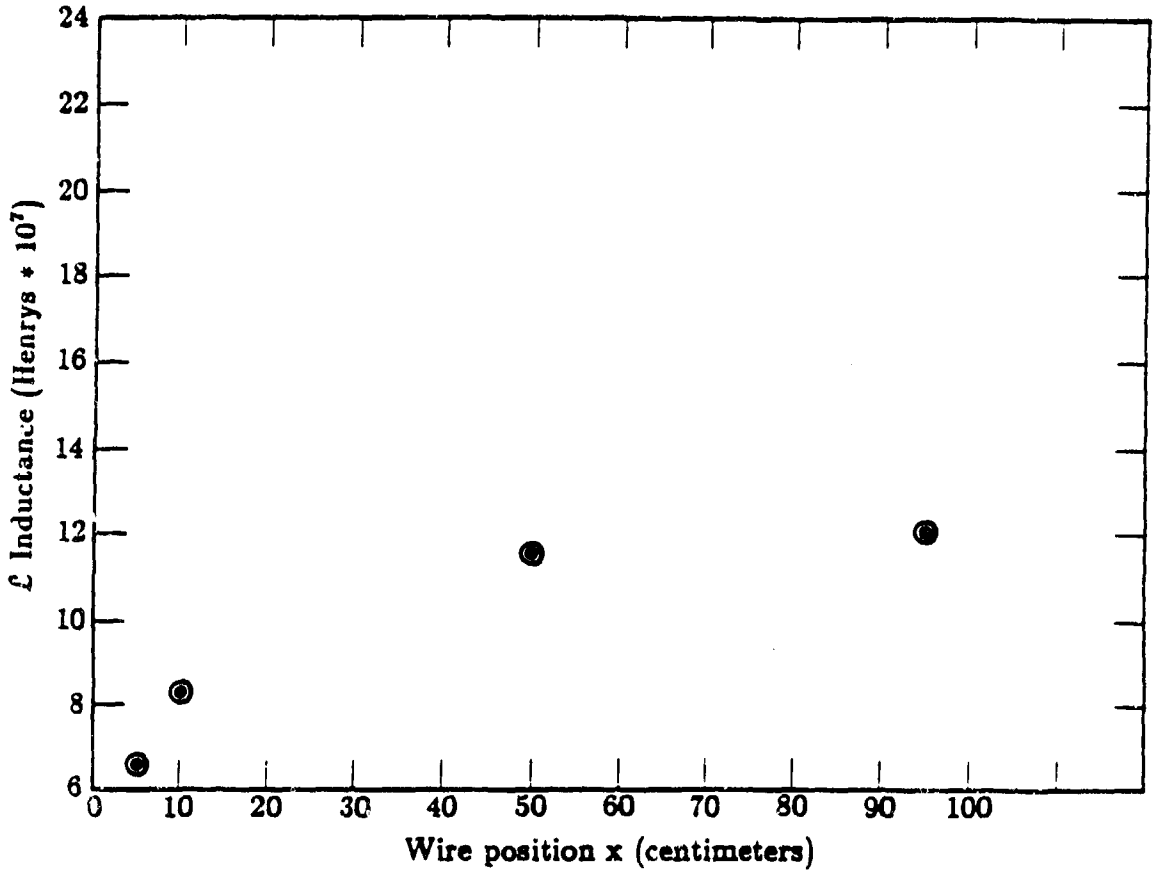

Figure A-5. Inductance as a function of wire position for table A-2 case.

$$\omega \gg \omega_1$$

equation A-2 shows the product of frequency and internal field remains a constant. Hence, the EMF and wire current are constant for frequencies above this value. Consequently, the maximum wire current occurs at frequencies slightly above ω_1. At much higher frequencies, of course, skin depth and other effects alter this behavior and reduce the wire current far below its maximum.

Equation A-12 indicates that the larger the wire resistance and inductance the smaller the wire current. At low frequencies

$$\omega \ll \frac{R}{\mathcal{L}}$$

the resistance will dominate the inductive reactance and the wire current will be ninety degrees out of phase with the internal magnetic field. At sufficiently high frequencies

$$\omega \gg \frac{R}{\mathcal{L}}$$

the resistance is negligible and the current is in phase with the internal field. As explained above if $\omega \ll \omega_1$ then the internal magnetic field is in phase with the external driving field and ninety degrees out of phase if $\omega \gg \omega_1$. The inductance can be approximated by that of a wire in free space although section A.4 derives a more accurate value.

The wire current can also be derived in the time domain. Substituting equation A-1 in equation A-2 yields

$$I(\omega) = \frac{i\omega G H^D(\omega)}{(R - i\omega\mathcal{L})(1 - i\omega/\omega_1)}$$

where

$$G = \mu_0 \left[xL - \frac{wL(L + 2x)}{2(w + L)} \right]$$

This is the wire current as a function of the external, driving magnetic field H^D in the frequency domain. By taking the inverse fourier transform the wire current I(t) as a function of time is found to be

$$I(t) = \frac{G\omega_1}{R - \mathcal{L}\omega_1} \int_0^t dt' H^D(t') \left\{ \frac{R}{\mathcal{L}} e^{-\frac{R}{\mathcal{L}}(t-t')} - \omega_1 e^{-\omega_1(t-t')} \right\}$$

This is the wire current as a function of time driven by an arbitrary external pulse whose time dependence is H^D (t).

Clearly, the wire current depends upon ω_1 and the characteristic frequency $R/\mathcal{L}$. The first is the cutoff frequency below which the enclosure shields the external field very poorly. The second is the time constant of the R - $\mathcal{L}$ circuit formed by the wire and the box. Fluctuations faster than ω_1 and $R/\mathcal{L}$ are smoothed out by this integral. In general, when the driver is first turned on the current slowly builds in the wire and after it is turned off the wire current slowly decays to zero.

The authors believe that the frequency domain solution in equations A-1, and A-2 and the above time domain solution contain the basic physics of the problem and permit reasonably accurate predictions in most situations. A straightfoward extension of the theory will enable predictions to be made for wires of any shape.

A.4 RESULTS AND BASIC PHYSICS

Figure A-2 illustrates a metallic enclosure driven by an external magnetic field directed along one of its edges and oscillating at the frequency ω. Because the wavelength is much longer than the box dimensions the field is independent of position. If the current on the internal wire can be predicted for this case then it can be predicted for any long wavelength external driving field. It is only necessary to fourier analyze the more complex driver into its frequencies and resolve the field at each frequency into its components along the three orthogonal edges. The total wire current is the sum of the currents produced by each part of the driver.

The electromagnetic field which is produced by the current within the wire obeys Faraday's and Ampere's laws

$$\nabla \times E^w = i\omega\mu_0 H^w$$

$$\nabla \times \mathbf{H}^w = \mathbf{J}^w - i\omega\epsilon_0\mathbf{E}^w$$

within the box where $\mathbf{J}^w$ is the current density in the wire. A single frequency is considered which,as explained above, is not a loss of generality. In this report all quantities are assumed to vary as exp(-i ω t). Within the walls having conductivity σ

$$\nabla \times \mathbf{E}^w = i\omega\mu_0\mathbf{H}^w$$

$$\nabla \times \mathbf{H}^w = \sigma\mathbf{E}^w - i\omega\epsilon_0\mathbf{E}^w$$

and outside the enclosure the fields satisfy both

$$\nabla \times \mathbf{H}^w = -i\omega\epsilon_0\mathbf{E}^w \qquad (A-13)$$

and Faraday's law.

The box is radiated with a driving field which, presumably, is produced by an external current density $\mathbf{J}^e$. The current density might, for instance, be the currents within a HPM microwave weapon or the Compton current in the atmosphere which generates an EMP pulse. $\mathbf{J}^e$ is assumed to be known. Outside the box the field produced by this driver satisfies Faraday's law and

$$\nabla \times \mathbf{H}^e = \mathbf{J}^e - i\omega\epsilon_0\mathbf{E}^e \quad .$$

In the walls the governing equation is

$$\nabla \times \mathbf{H}^e = \sigma\mathbf{E}^e - i\omega\epsilon_0\mathbf{E}^e$$

and within the box

$$\nabla \times \mathbf{H}^e = -i\omega\epsilon_0\mathbf{E}^e \qquad (A-14)$$

The presence of the wire is correctly omitted in equation A-14

The total electric E_T and magnetic H_T fields are the sum of the fields produced by the external driver J^e, the current in the wire J^w and the current in the walls σE_T

$$E_T = E^w + E^c$$

$$H_T = H^w + H^e$$

However, the wire current J^w is caused by the total electric field according to

$$J^w = \sigma^w (E^w + E^e) \qquad (A-15)$$

in terms of the wire conductivity, σ^w. Solving equations A-13 through A-15 furnishes the current J^win the wire. The wire current derived in this way is exact but it is difficult to solve the equations if the wire is so thick that the current around it is non-uniform. The authors will attempt this less important case in the future.

This approach to the problem which was pointed out by Dr James Gilbert at Mission Research Corporation is similar to the technique used to solve many scattering problems. Solving equations A-13 yields the electromagnetic fields produced by a specified wire current J^w when the external driver J^e is not present. Solving equations A-14 yields the electromagnetic fields due to the known external driver J^e when the wire is not present. These two simpler problems are solved in sections A.3 and A.4. Equation A-15 then yields the wire current trivially. Of course, in equation A-15 E^w is a function of the unknown J^w. So 2-3 is actually an implicit equation which must be solved to find J^w. The authors employed this method to derive the wire current results in the previous section.

The electric field can be written in terms of the scalar and vector potentials[3], ϕ and A

$$E^w = i\omega A^w - \nabla \phi^w$$

$$E^e = i\omega A^e - \nabla \phi^e \qquad (A-16)$$

Integrating equation A-15 along the wire (figure A-2) yields

$$IR = \int_A^B E^w + E^e dx = \phi_A^w - \phi_B^w + \phi_A^e - \phi_B^e + i\omega \int_A^B A^w dx + i\omega \int_A^B A^e dx \qquad (A-17)$$

where R is the wire resistance.

Consider the integration path through the walls shown in figure A-2. The line integral of the electric field along this path is called

$$V_d = \int E_T d\ell = \phi_B^w - \phi_A^e + i\omega \int A^w d\ell + i\omega \int A^e d\ell \qquad (A-18)$$

adding equation A-17 and equation A-18 yields

$$IR + V_d = i\omega \oint A^w d\ell + i\omega \oint A^e d\ell \qquad (A-19)$$

Where the closed path is formed by the wire and the path through the walls. But the line integrals can be related to the surface integral of the magnetic field through the closed path

$$\oint A \cdot d\ell = \int (\nabla \times A) \cdot ndS = \int B \cdot ndS$$

by Stokes theorem yielding

$$IR + V_d = i\omega \int B^w \cdot ndS + i\omega \int B^e \cdot ndS \qquad (A-20)$$

This is a rigorous proof of equation A-9, the starting point for the approximate wire treatment in section A.1. It is important to note that in adding equation A-17 and equation A-18 the scalar potentials drop out. Consequently, equation A-20 is correct even in the general case for which the scalar potential is not negligible. Calculating the wire current with this equation requires that V_d be estimated, however, a complication which is avoided in the following manner.

The scalar potentials are small and can be neglected in equation A-17. This is shown in sections A.3 and A.4 and explained intuitively in the following way. In the

Lorentz gauge the scalar and vector potentials are driven by the charge ρ and current density $\overline{J}$, respectively[3]

$$\nabla^2\phi - \frac{1}{c^2}\frac{\partial^2\phi}{\partial t^2} = -\frac{1}{\epsilon_0}\rho$$

$$\nabla^2\overline{A} - \frac{1}{c^2}\frac{\partial^2\overline{A}}{\partial t^2} = -\mu_0\overline{J}$$

In general, charge accumulates on the surface of the wire and creates an scalar potential whose gradient is the irrotational part of the electric field. The charge accumulates in such a way that the boundary condition (equation A-15) is satisfied on the wire. For instance, if the wire is coiled on a cylinder to form an inductor then a small charge density is deposited by the almost divergenceless wire current on the surface. For a zero resistance wire the field on its surface must be zero so the electric field $i\omega A$ must be equal and opposite to that produced by the scalar potential $\nabla\phi$. In a small number of very symmetrical situations, however, the vector potential alone is sufficient to satisfy the boundary condition.

Consider, for example, a zero resistance wire loop in a homogeneous oscillating magnetic field (figure A-6) which induces an EMF around the wire and causes a current to flow. The oscillating current creates an electric field $i\omega A$ at the wire which just cancels the induced field. It is easily shown that charge does not accumulate along the thin wire and the scalar potential is zero. But if the circular loop is distorted slightly then the vector potential can not by itself zero the electric field and a scalar potential must be produced. Similarly, if the oscillating driving field is not homogeneous the scalar potential is significant.

The vector potential A^e is the sum of the potentials produced by the current in the walls A^c and the external source A^d. The low frequency external source produces a homogeneous magnetic field H^D directed along the z axis (figure A-2) so that

$$H_D = \frac{1}{\mu_0}\nabla \times \overline{A}^D$$

Since the vector potential is symmetrical about an axis through the center of the box parallel to the z axis the correct solution to this equation is

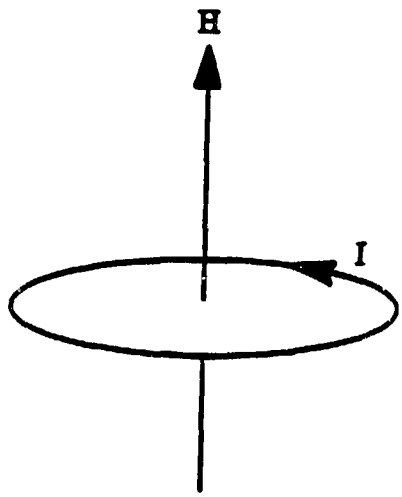

Figure A-6. Wire in an oscillating magnetic field.

$$A_x^D = \frac{-\mu_0}{2}(y - \frac{b}{2})H_D$$

$$A_y^D = \frac{\mu_0}{2}(x - \frac{a}{2})H_D \qquad (A-21)$$

Hence, equation A-17 becomes

$$IR = i\omega \int_A^B A^w dx + i\omega \int_A^B A^c dx + i\omega \int_A^B A^D dx \qquad (A-22)$$

This final equation, rather than equation A-17, is used to find the wire current with the code.

In summary, the method which the authors developed to calculate accurately the wire current employs the computer code discussed in section A.3 to calculate

$$\int_A^B A^w dx$$

and the analytic calculation in section A.4 to yield

$$\int_A^B A^c dx$$

Then equation A-21 yields

$$\int_A^B A^D dx$$

Since the magnetic field is proportional to the wire current I

$$\int_A^B A^w dx = \mathcal{L} I \qquad (A-23)$$

Finally, the wire current is obtained by solving the algebraic equation A-22 which becomes

$$IR + i\omega \mathcal{L} I = i\omega \int_A^B A^c dx + i\omega \int_A^B A^D dx \qquad (A-24)$$

It is worthwhile pointing out that $\mathcal{L}$ is the inductance of the wire in the enclosure in the limit that the walls shield the outside of the box from the wire very effectively. This equation differs from equation A-20 which is the starting point of the analytic method in two ways. Firstly, it is not necessary to calculate V_d, the line integral of the electric field in the walls. Secondly, the scalar potential has been neglected in equation A-23 but it is included in the surface integrals in equation A-20.

A.5 EXTERNAL DRIVER CALCULATION

In this section the electric field produced at the wire by the external magnetic field which diffuses through the shield is derived. Outside the wall the magnetic intensity H can be expressed[4] by the gradient of a magnetic scalar potential Ω

$$H = \nabla\Omega$$

where

$$\nabla^2\Omega = 0 \quad .$$

It is well known[3] that within the enclosure the scalar potential can be expressed as a function of its value and derivative on the inside surface of the wall

$$\Omega^{in}(\bar{r}) = \int (G\frac{\partial\Omega^{in}}{\partial n'} - \frac{\partial G}{\partial n'}\Omega^{in})dS' \qquad (A-25)$$

where

$$G = \frac{1}{4n}\frac{1}{|r-r'|}$$

Similarly, outside the rectangle

$$\Omega^{out}(\bar{r}) = \Omega^{ex}(\bar{r}) - \int (G\frac{\partial\Omega^{out}}{\partial n'} - \frac{\partial G}{\partial n'}\Omega^{out})dS' \qquad (A-26)$$

where the normal derivative is always outside the box and Ω^{ex} is the external field imposed on the metallic enclosure by the source such as a low frequency electromagnetic wave.

The current in the thin walls is expressed as a surface current density $\overline{K}$ (amperes/meter) parallel to the conducting surface. Assuming it is divergenceless permits it to be expressed in terms of a scalar stream function ψ

$$\overline{K} = \bar{n} \times \nabla_s\psi \qquad (A-27)$$

where n is the surface normal and the surface divergence is ∇_s.

Latham and Lee[4] have shown the magnetic scalar potentials on the inside and outside surfaces of the walls obey

$$\frac{1}{2}\Omega^{in} = -\int \Omega^{in}\frac{\partial G}{\partial n'}dS' + \frac{1}{i\omega\mu_0 g}\int G\nabla_s'^2\psi dS'$$

$$\frac{1}{2}\Omega^{out} = \Omega^{ex} + \int \Omega^{out}\frac{\partial G}{\partial n'}dS' - \frac{1}{i\omega\mu_0 g}\int G\nabla_s'^2\psi dS' \qquad (A-28)$$

where $g = \sigma\Delta$, the product of wall conductivity and thickness.

Making use of the facts that the normal derivative of H is continuous across the wall whereas the jump in the tangential component of H across the wall is equal to the surface current density K yields an equation for the stream function[4]

$$\frac{1}{4}\psi(r) = \int G\frac{\partial\Omega^{ex}}{\partial n'}dS' + \int\int \psi(r''\frac{\partial G}{\partial n''}\frac{\partial G}{\partial n'}dS'dS''$$

$$-\frac{1}{i\omega\mu_0 g}\int(\psi(r') - \psi(r)\nabla_s' G dS' \qquad (A-29)$$

This integral equation is ideally suited to numerical solution since only integrals over the unknown ψ rather than derivatives appear. The function ψ is calculated at a several hundred locations on the surface of the box. For the i^{th} location the integral equation is approximated by

$$\frac{1}{4}\psi_i = \sum_j G\frac{\partial\Omega^{ex}}{\partial n'}\delta^2 + \sum_j\sum_k \psi_k\frac{\partial G}{\partial n_k}\frac{\partial G}{\partial n_j}\delta^4$$

$$-\frac{1}{i\omega\mu_0 g}\sum_j(\psi_j - \psi_i)\nabla_s'^2 G\delta^2$$

where δ^2 is the area of each surface cell. This yields a system of several hundred simultaneous linear algebraic equations which are then solved numerically with the code BOX4 to yield the stream function. Once, ψ is known the magnetic scalar potential Ω and the magnetic field can be calculated within the box with little additional difficulty. Furthermore, the magnetic vector potential A at the wire produced by the current in the walls can be found by integrating over the stream function

$$A^c = \mu_0 \int dS' G(n \times \nabla_s \psi) \qquad (A-30)$$

This is the quantity needed in section A.4 (equation A-24) to calculate the wire current.

The numerical solution is fast and reasonably accurate. In the high frequency limit the walls shield the external magnetic field very well. Consequently, the magnetic vector potential A^D (section A.4) produced by the known driver is equal and opposite to that produced by the wall current (equation A-30). In the figure A-3 example they differed by only eight percent when ψ was approximated by 96 cells. This accuracy was achieved for a total computer cost of about fifty cents. Dividing the box into 216 cells achieved slightly better accuracy for a cost of about ten dollars. The computations were done on an ELXSI time-sharing computer which is similar to the popular Digital Equipment Corporation VAX780. Most of the computer time is spent evaluating the coefficients in the simultaneous equations many of which are multiple integrals rather than actually solving the equations which is done by the Gaussian elimination method. A significant savings in computer cost could be realized by making better use of the problem's symmetry when computing the multiple integrals.

An important simplification is understood by examining the limit of equation A-28 as the frequency becomes much larger than ω_1. Then the last terms in these equations are small and to zero order the internal field Ω^{in} is zero since the walls shield well at high frequencies. Equation A-28b yields a zero order approximation to the external potential Ω^{out} which can be substituted back into equation A-28a to yield a better estimate for the internal field

$$\frac{1}{2}\Omega^{in}(\bar{r}) + \int \Omega^{in}(\bar{r}) \frac{\partial G}{\partial n} dS' = \frac{1}{i\omega\mu_0\sigma\Delta} \int G \nabla^2 \Omega^{out} dS'$$

The scalar potential Ω^{in} is a function of frequency and position $\bar{r}$. But the frequency appears only in the coefficient of the right hand member. Consequently, as the frequency is increased the field Ω^{in} at each location decreases inversely with the frequency. Hence, the vector potential A^e decreases at the wire inversely with frequency. As was pointed out in section A.1 this has important consequences.

The assumption that the wall current is divergenceless implies that there is no charge accumulation on the walls. Therefore, the scalar potential ϕ must (under this assumption) be zero. As explained in section A.4, usually, this is not true. In this approach

it is impossible to calculate the contribution to the electric field produced by the scalar potential. Fortunately, BOX4 shows that the vector potential A^c produced by the wall current is approximately constant along the wire. Section A.6 indicates that the potential produced by the wire A^w is also constant. But the total electric field on the wire must be constant since it equals IR. Since A^c and A^w are constant they are sufficient to satisfy the boundary condition on the wire and ϕ must be negligibly small.

Toward the edges of the wire A^c is not constant. The authors believe this is due to numerical inaccuracy. Further attention to this point is necessary.

A.6 WIRE CURRENT

As the oscillating current flows through the wire and around the walls of the enclosure it produces a substantial electric field. If the wire resistance is zero, the magnitude of the field (along the wire) which penetrates the enclosure is equal to that of the field produced by the wire current. In this section the fields produced in the box by the wire current are calculated so that the integral in equation A-23 and the inductance can be evaluated.

Figure A-1 illustrates a rectangular enclosure driven by a current I which runs through its central wire and returns via the metallic walls. The current oscillates at the frequency ω at a constant amplitude. It is not necessary to specify the source of energy which drives the current against the ohmic losses in the walls and the wire. In the limit of very low frequency, small conductivity or small wall thickness the current will distribute itself so that the electric field at the walls is sufficient to drive the current. In general, appreciable magnetic fields will leak outside the enclosure. But as the conductivity or wall thickness increase the electric field at the walls decrease. Furthermore, as the frequency increases the electric field induced within the enclosure by the changing current becomes much larger than that necessary to drive the wall current. In either limit the boundary condition at the walls is that the electric field at the walls becomes negligible. Consequently, the wall conductivity can be considered infinite. The conditions for which this idealization is valid are quantified at the end of this section. In the case of the conductivity and wall thickness referred to in the section A.1 examples the approximation is justified for frequencies above about one kilohertz.

The vector potential within the infinite conductivity box satisfies

$$\nabla^2\overline{A} + \frac{\omega^2}{c^2}\overline{A} = -\mu_0\overline{J} \qquad (A-31)$$

which has the solution

$$\overline{A} = \int G(\bar{r}, r\prime)JdV$$

where the Green's function satisfies the appropriate boundary conditions on the walls. J is the wire current density. In terms of the eigenfunctions satisfying the Helmholtz equation

$$\nabla^2\psi_n + \left(\frac{\omega^2}{c^2} + \frac{\omega_n^2}{c^2}\right)\psi_n = 0 \qquad (A-32)$$

the Green's function[3] is

$$G = \mu_0 c^2 \sum_n \frac{\psi_n^*(r')\psi_n(r)}{\omega_n^2 - \omega^2} \qquad (A-33)$$

Equation A-33 indicates that if the frequency ω is much less than the natural modal frequencies of the box ω_n then the vector potential does not differ appreciably from the value if would have if $\omega = 0$. Consequently, it is only necessary to solve the quasi-static equation

$$\nabla^2\overline{A} = -\mu_0 J$$

subject to the boundary conditions that the normal component of the magnetic field on the wall is zero. The eigenfunctions are then

$$\psi_{mn} = \sqrt{\frac{8}{abc}}\sin(\frac{m\pi y}{b})\sin(\frac{n\pi z}{c})$$

$$\frac{\omega_{mn}^2}{c^2} = (\frac{m\pi}{b})^2 + (\frac{n\pi}{c})^2$$

and the vector potential is

$$A_x = \frac{8\mu_0 I}{bc\pi^2} \sum_{\ell,1m=1}^{\infty} \frac{\sin(\frac{m\pi\xi}{b})\sin(\frac{n\pi\eta}{c})}{(\frac{\ell}{a})^2 + (\frac{m}{b})^2} \sin(\frac{m\pi y}{b})\sin(\frac{n\pi z}{c})Q_{mn} \qquad (A-34)$$

where the wire position is $y = \xi$ and $z = \eta$ and

$$Q_{mn} = \exp\left\{-(\frac{\pi w}{2})^2\left[(\frac{m}{b})^2 + (\frac{n}{c})^2\right]\right\} \quad .$$

It is important to consider a wire of finite radius to calculate the wire inductance. Furthermore, the series converges very poorly if the wire radius is zero since this necessitates very high order spatial modes because the vector potential changes direction across the wire. In this report the wire current density J has been assumed to fall off as a Gaussian with characteristic wire radius w_0

$$J = \frac{I}{\pi w^2} e^{-(\frac{y-\xi}{w_0})^2} e^{-(\frac{z-\xi}{w_0})^2}$$

From the above series expression for A the magnetic flux through the contour in figure A-2 can be derived

$$\int (\nabla \times A \cdot n) dS$$

It is the negative of the electromotive force produced around the loop by the wire current. Since the walls are infinitely conducting it is also equal to

$$EMF = i\omega \int_A^B A \cdot dx \qquad (A-35)$$

These are the final expressions needed in section A.4 (equation A-23) to calculate the wire current. The inductance $\mathcal{L}$ is defined in terms of this integral by equation A-23.

The circumstances for which the infinite conductivity approximation is valid are easily quantified. The resistance of a conducting sheet whose length and width are equal is

$$R_w = \frac{1}{\sigma \Delta} \qquad (A-36)$$

where σ and Δ are the conductivity and thickness. For instance, a sheet of conductivity 10^6 mho/m and one millimeter thickness has a resistance of 0.001 ohms. Clearly, if an ohm meter is used to measure the resistance of the walls between points A and B (on figure A-2) a resistance of this order of magnitude will be observed provided the wall conductivity and thickness are the same as the sheet and the box's length, width and height are comparable. The line integral of the electric field in the wall from point A to B is path dependent but is typically of the order IR_w in terms of the wire current I. The EMF around the entire loop in figure A-2 is shown in expression A-35. The infinite conductivity approximation is valid if the EMF greatly exceeds IR_w or

$$IR_w \ll \omega \int_A^B A \cdot dx \qquad (A-37)$$

It has been assumed in equation A-35 that the contribution to the electric field due to the scalar potential is negligible. It is easily seen from equation A-35 that

$$\nabla \cdot A = 0$$

Consequently, from the Lorentz condition the scalar potential is also zero. Therefore, for frequencies much lower than the modal frequencies of the enclosure (frequently below hundreds of megahertz) but sufficiently high that the walls provide reasonable magnetic field shielding (frequently above one kilohertz) the scalar potential causes little electric field. Hence, there is no charge in the system and the flow of current is divergenceless. It is important to understand that at higher frequencies the scalar potential can not be neglected. Furthermore, the straight wire is a particularly simple case. If the wire were to lead to a circuit containing inductors or capacitors then these would produce a scalar potential. If these circuit components occupied a large fraction of the volume of the box the computer approach taken in this report would require modification.

The inductance has not been carefully computed at low frequencies whre equation A-37 is not valid.

A.7 CALCULATION OF HIGH FREQUENCY RESPONSE

In the previous sections we have described in detail our work on computation of the low frequency response of the wire, in particular the solution of the interior potential equation, including the wire. In this section we shall discuss the problem of high frequency response calculations. Since the low frequency solution was the main thrust of our early efforts the progress here has been more limited. To date we have almost completed the development of the code.

The surface current on a box illuminated by electromagnetic radiation can be described[5] in terms of the incident magnetic fields. A careful analysis[5], yields the equation:

$$\vec{K}(\vec{r}) - 2\int \hat{n} \times \vec{K} \times G(\vec{r},\vec{r}')ds' = 2\vec{H}^{ext}(\vec{r}) \qquad (A-38)$$

where K is the surface current, $\vec{H}^{ext}$ is the external magnetic field and G is the outgoing Green function

$$G(\vec{r},\vec{r}') = 1/\{4\pi|\vec{r}-\vec{r}|\exp(ik|\vec{r}-\vec{r}'|)\} \qquad (A-39)$$

corresponding to frequency w = k c.

The above equations provide the current density on the surface of the box. Reference 1 indicates how these are used to drive the internal fields and wire current.

In our first effort we have focussed on the solution of equation A-38, i.e. the determination of the surface current density on the outside of the box. Before we proceed to discussion of the numerical solution of the problem we note that "high frequency" in our case usually indicates frequencies of 1 MHz and higher. Since the integral in equation A-38 is oscillatory in nature, the required number ofsteps for the calculations is dictated by the standard assumption of 10 – 20 points per period.

To solve the problem numerically we have adopted the standard gridding of the box faces as indicated in our solution of the low frequency problem. For a system of equations to have a meaningful result typical matrix dimensions should not exceed 1000 × 1000 or so. This limits the number of cells on each face to 42 or about 6 cells in each direction. This implies that our solution will be quite accurate for a box whose size is

smaller than about third of a wavelength. For the 1 MHz frequency, this corresponds to boxes of about 100 meters across.

For larger boxes, the solution will naturally be less accurate and we shall use our code to provide an initial estimate of the surface current. This solution will be improved upon by inserting it into a very accurate integrator of the LHS of equation A-38 and comparing with the RHS driver. Such integrator is not constrained by memory requirements and does not include any matrix operations.

We expect these two codes will be sufficient to provide a general trend prediction for the solutions computed but we are aware that the solution accuracy is going to be limited. However, since our goal is to dévelop simple models of surface currents, we feel that the finite difference approach should be adequate. Furthermore the accurate integration of the LHS of equation A-38, once coded, will provide a test method for evaluation of models of the surface current density.

After expansion of the vector product and if we replace the integral by a sum, the integral equation becomes a matrix equation for the surface currents. For the present problem we have considered only a rectangular box. Other box geometries could be also computed but the algebra becomes somewhat more involved. For the six faces of the box, there are 12 independent components of the current together with the boundary conditions at the edges of the box which arise from continuity. Each component is complex and the physical current is the real part of the product K exp(iwt).

The resultant matrix equation can be cast in the form:

$$\underline{A}\,\underline{J} = \underline{D}$$

where A is the LHS matrix (kernel) and D is the driving term. In order to save memory, we had hoped that the kernel has some inherent symmetries that permit more efficient computation. However, as it turns out, the matrix A is band structured, but not symmetric (or antisymmetric). Thus the computation of the surface currents requires large memory to be available.

Currently, the coding is essentially completed, with some problems occurring with the mixing of real and complex arithmetics. We expect to have some results within the next couple of weeks. We shall spend a significant amount of time verifying the code results for the limiting cases.

The next stage of our calculations, solving the Maxwell equations in the box interior can be accomplished with codes already available. This effort is expected to be relatively straightforward.

Our next task is the development of approximate formulas for the surface currents. While it is possible to rely solely on numerical experiments we are also conducting an analysis of the structure of the solution and a survey of the literature for available exact solution in special geometries.

Distribution

Administrator
Defense Technical Information Center
Attn: DTIC-DDA (2 copies)
Cameron Station, Building 5
Alexandria, VA 22304-6145

U.S. Army Research Laboratory
Attn: AMSRL-OP-CI-AD, Library (3 copies)
Attn: AMSRL-OP-CI-AD, Mail & Records Mgmt

REPORT DOCUMENTATION PAGE

Form Approved
OMB No. 0704-0188

1. AGENCY USE ONLY *(Leave blank)*	2. REPORT DATE	3. REPORT TYPE AND DATES COVERED
	April 1993	Final, 9/87–4/88

4. TITLE AND SUBTITLE
Electromagnetic Diffusion and Wire Coupling

5. FUNDING NUMBERS
Project No.: EE17EB

6. AUTHOR(S)
Bart Goldstein and Rudolf Goldflam

7. PERFORMING ORGANIZATION NAME(S) AND ADDRESS(ES)
Mission Research Corporation
735 State Street
P.O. Drawer 719
Santa Barbara, CA 93101

8. PERFORMING ORGANIZATION REPORT NUMBER
MRC-R-1156

9. SPONSORING/MONITORING AGENCY NAME(S) AND ADDRESS(ES)
U.S. Army Research Laboratory
2800 Powder Mill Road
Adelphi, MD 20783

10. SPONSORING/MONITORING AGENCY REPORT NUMBER
ARL-CR-54

11. SUPPLEMENTARY NOTES
Contract No.: DAAL02-87-C0113
ARL contact: Ronald Chase

12a. DISTRIBUTION/AVAILABILITY STATEMENT
Approved for public release; distribution unlimited.

12b. DISTRIBUTION CODE

13. ABSTRACT *(Maximum 200 words)*

This report documents the research performed to develop physical insight into the coupling of radiated, pulsed, electromagnetic energy to a thin wire located inside a rectangular metallic enclosure. The electromagnetic fields diffuse into the rectangular cavity. The cavity size is not small compared to the wavelengths in the exciting field. A prime objective was to determine how the wire transients will change due to the parameters of cavity size, wire locations and orientation, and incident pulse parameters such as polarization, risetime, and decay time.

The approach involved frequency domain analysis based on three distinct frequency regimes: low, intermediate, and high. In the low frequency region the skin depth is larger than the wall thickness of the enclosure. The intermediate region extends to the lowest internal mode of the enclosure. The high frequency region extends upward from the lowest mode. Validation of the analytical results, planned under Phase II of the SBIR, were not performed.

14. SUBJECT TERMS	15. NUMBER OF PAGES
EMP, electromagnetic coupling, shielding, diffusion, wire coupling	101
	16. PRICE CODE

17. SECURITY CLASSIFICATION OF REPORT	18. SECURITY CLASSIFICATION OF THIS PAGE	19. SECURITY CLASSIFICATION OF ABSTRACT	20. LIMITATION OF ABSTRACT
Unclassified	Unclassified	Unclassified	UL

NSN 7540-01-280-5500

Standard Form 298 (Rev 2-89)
Prescribed by ANSI Std Z39-18
298-102